

Polarons and Charge Localization in Metal-Halide Semiconductors for Photovoltaic and Light-Emitting Devices

Leonardo R. V. Buizza and Laura M. Herz*

Metal-halide semiconductors have shown excellent performance in optoelectronic applications such as solar cells, light-emitting diodes, and detectors. In this review the role of charge–lattice interactions and polaron formation in a wide range of these promising materials, including perovskites, double perovskites, Ruddlesden–Popper layered perovskites, nanocrystals, vacancy-ordered, and other novel structures, is summarized. The formation of Fröhlich-type “large” polarons in archetypal bulk metal-halide ABX_3 perovskites and its dependence on A-cation, B-metal, and X-halide composition, which is now relatively well understood, are discussed. It is found that, for nanostructured and novel metal-halide materials, a larger variation in the strengths of polaronic effects is reported across the literature, potentially deriving from variations in potential barriers and the presence of interfaces at which lattice relaxation may be enhanced. Such findings are further discussed in the context of different experimental approaches used to explore polaronic effects, cautioning that firm conclusions are often hampered by the presence of alternate processes and interactions giving rise to similar experimental signatures. Overall, a complete understanding of polaronic effects will prove essential given their direct influence on optoelectronic properties such as charge-carrier mobilities and emission spectra, which are critical to the performance of energy and optoelectronic applications.

1. Introduction

The rise of metal-halide perovskites for photovoltaic applications over the last decade has been rapid and successful. These materials have shown a range of outstanding optoelectronic properties ranging from excellent optical absorption,^[1] to tunable bandgaps,^[2] high electron and hole mobilities,^[3] and long charge-carrier diffusion lengths.^[4] These properties have enabled metal-halide perovskite (MHP) solar cells to achieve power conversion efficiencies above 25%, rivaling the laboratory record for commercially ubiquitous silicon solar cells, and even surpassing

29% when used in tandem silicon-MHP solar cells.^[5] More recently, a new range of related metal-halide semiconducting materials has emerged, many of which exhibit similarly advantageous properties; these materials are not perovskites, but often share aspects of the crystal structure, such as octahedral geometries, or have similar chemical compositions, notably the inclusion of halide elements.^[6–8] So far, investigations have included layered Ruddlesden–Popper perovskites,^[8,9] vacancy-ordered perovskites,^[10] double perovskites,^[11] and quasi-0D metal-halides.^[12] Applications for these metal-halide semiconductors range from solar cells^[1] to thermoelectrics,^[13] and gamma-ray detectors^[14] to LEDs.^[8] Understanding whether charge carriers in a material recombine radiatively or not, whether they move without encountering obstacles, or whether they can be extracted easily can determine the success of one composition over another when innovative materials for such applications are explored. Thus, in order to predict the suitability of any of these materials for specific optoelectronic applications,

a clear understanding of the dynamics of charge carriers, and of their interaction with the crystal lattice, is critical. A fundamental type of charge–lattice interaction manifests as a polaron, which forms when a photoexcited electron or hole interacts with the ions in a polarizable crystal, leading to a displacement in ionic positions. The displaced ions can then couple to the original charge carrier, and the overall lattice polarization along with the charge are considered as a single entity, a polaron,^[15,16] with the typical effect being that charge-carrier motion is impeded as the lattice distortion moves throughout the lattice along with the charge carrier.^[17,18]

The use of new metal-halide materials in solar cells illustrates the links between materials selection, a fundamental understanding of charge–lattice couplings, and innovation in optoelectronics. Initial research focused on the metal-halide perovskite $MAPbI_3$ ($MA = CH_3NH_3$),^[1] but has now shifted to more complex, multi-cation MHPs and hybrid 2D–3D perovskites that provide better stability and enhanced crystallinity.^[19,20] Alongside this shift, a thorough understanding of the role of large polarons in MHPs developed,^[21,22] providing crucial insights into the costs and benefits of charge–lattice interactions for device applications.^[23–25] Notwithstanding this improved understanding, there is still broad scope for the

L. R. V. Buizza, Prof. L. M. Herz

Department of Physics

University of Oxford

Clarendon Laboratory, Parks Road, Oxford OX1 3PU, UK

E-mail: laura.herz@physics.ox.ac.uk

Prof. L. M. Herz

TUM Institute for Advanced Study (IAS)

Lichtenbergstraße 2 a, Garching bei München 85748, Germany

 The ORCID identification number(s) for the author(s) of this article can be found under <https://doi.org/10.1002/adma.202007057>.

DOI: 10.1002/adma.202007057

exploration of new materials beyond MHPs. The desire to avoid the use of toxic lead,^[26] adjusting bandgaps to suit tandem solar cell,^[27–29] the introduction of nanostructuring or variation of crystal structures to tailor optoelectronic properties,^[2,30] and the push to make use of more stable fully inorganic compositions^[31] all open new avenues for the exploration of novel materials and compositions.

As research has moved beyond MAPbI₃ toward other materials, the need to understand the impact of charge–carrier interactions has remained as pressing as ever. For photovoltaics, large polarons appear not to be significantly detrimental, lowering charge-carrier mobilities and introducing some moderate couplings to the lattice but still allowing for efficient charge extraction.^[21,22,32,33] On the other hand, small polarons that limit charge-carrier mobilities substantially and lead to charge-carrier self-trapping and fast non-radiative recombination are clearly detrimental for photovoltaics.^[11,17,34] However, if self-trapped charges lead to broadband, efficient white-light emission, small polarons could be quite beneficial for solid-state lighting,^[8,35] as well as other applications such as gamma-ray detection.^[14,36] Recent reviews have emphasized the potential promise of metal-halide semiconductors in lighting applications^[37–39] and for radiation detection,^[40,41] but there has been little focus on the fundamental understanding of polaronic effects and charge localization, which affect the performance of these materials in devices. Thus, understanding the role of charge–lattice interactions is critical in ensuring that new materials for energy innovation are designed rationally and tailored appropriately to specific applications.

In this review, we summarize the state of current understanding of charge-carrier localization and the role of polarons in a range of metal-halide semiconductors. First, we outline the evolution of polaron theory and its application to metal-halide perovskites, before covering briefly a variety of experimental approaches that can be useful for observing and understanding the role of polarons in semiconducting materials. We then explore a variety of material classes, starting with archetypal bulk 3D MHPs and moving on to nanocrystal MHPs, double perovskites, Ruddlesden–Popper perovskites, and a range of novel metal-halide semiconductors. In each case we outline the current understanding of the role of polarons and interactions between charge carriers and the lattice. As we discuss throughout, polaron formation and charge-carrier localization in metal-halide semiconductors relies on three complementary factors: the chemical composition of the material, the dimension of the material (both structural and electronic, as discussed below), and the ease of structural distortions in the material. Finally, we provide a brief outlook, covering some questions that remain unanswered and potential new avenues of research.

2. Polaron Theory: A Brief Introduction

2.1. The “Large” Polaron of Landau and Fröhlich

As a guide for the remainder of this perspective, we provide a short outline of the development of theories to describe polarons and provide a useful framework in which to consider the formation of large and small polarons. An initial theoretical

description of polarons was provided by Landau in 1933,^[15] and later work with Pekar showed how polarons alter the effective mass of charge carriers moving in crystals.^[16,42] Fröhlich, Pelzer, and Zienau subsequently developed a quantum mechanical description of polaron theory, introducing electron–phonon couplings in the place of the interaction between a charge carrier and a polarizable continuum.^[43] Solutions to their Hamiltonian were then provided by Fröhlich,^[44] Feynman,^[18] Hellwarth,^[45] Ōsaka^[46,47] and others in order to describe a range of electron–phonon interaction strengths,^[48] focusing specifically on couplings of charges to the macroscopic local electric fields generated by longitudinal-optical (LO) phonons in ionic crystals. This approach describes ‘large’ polarons for which the interactions are long-range, covering dozens of unit cells, and localization effects and changes in charge-carrier dynamics are less pronounced.^[49]

The original Fröhlich Hamiltonian describes a free electron interacting with a single, dispersionless LO phonon.^[43,44] Within this theory one can consider the dimensionless parameter α_F , which is used to quantify the strength of the interaction between the charge and the LO phonon:

$$\alpha_F = \left(\frac{1}{\epsilon_\infty} - \frac{1}{\epsilon_{\text{static}}} \right) \left(\frac{R_y}{\hbar\omega_{LO}} \right)^{1/2} \left(\frac{m^*}{m_e} \right)^{1/2} \quad (1)$$

where $R_y = 13.606$ eV is the Rydberg constant, ω_{LO} is the LO phonon frequency, and $\frac{m^*}{m_e}$ is the ratio of charge-carrier effective mass to the free electron mass. Further, ϵ_∞ and ϵ_{static} are the high-frequency and static limits of the dielectric function with respect to ω_{LO} , typically approximated as the values in the optical and THz frequency ranges, respectively.^[50] This parameter is of great value, as m^* , ω_{LO} , ϵ_∞ and ϵ_{static} can all be measured or calculated for a material, allowing direct evaluation of the coupling strength, as has been done for some semiconducting perovskite materials (see below and **Table 1**),^[22,32] often making use of formulations by Feynman and Hellwarth.^[45,51] Once the value of α_F is known, it can conveniently be used to calculate the polaron effective mass through $m_p = m^* \left(1 + \frac{\alpha_F}{6} + \frac{\alpha_F^2}{40} + \dots \right)$, an approximation first proposed by Feynman.^[18] Further, one can also use the Feynman and Hellwarth^[45,51] formulation to calculate polaron mobilities, as has been done by Sendner et al. for bulk 3D lead-halide perovskites.^[22] However, there are some limits to the applicability of the Fröhlich description; for example, its simplified assumption of a purely harmonic lattice potential^[44] may reduce accuracy for soft MHPs that are expected to exhibit stronger anharmonicities.^[24,52,53]

2.2. The “Small” Polaron

Holstein developed an approach for describing short-range interactions that lead to strong charge localization, and these situations are referred to as “small” polarons as they are typically limited to approximately a single lattice site.^[17] Landau originally suggested that, in cases with strong charge–lattice couplings and slow-moving charges, charge carriers might become immobilized, and thus be described as “self-trapped,”^[15] a state which has since been described in much

Table 1. Summary of measurements or calculations of the Fröhlich coupling parameter α_F , polaron effective mass m_p (in terms of its increase with respect to the band effective mass m^*), room-temperature charge-carrier mobility μ and power-law exponent p for the temperature-dependence of the mobility, across a variety of bulk metal-halide perovskite and related materials.

Reference	Material	Theoretical or Experimental	Approach	α_F	m_p (% boost relative to band effective mass)	μ ($\text{cm}^2 \text{V}^{-1} \text{s}^{-1}$ at room temperature)	p (from $\mu \propto T^p$)
Frost ^[21]	MAPbI ₃	Theoretical	Single-phonon Fröhlich model	2.39 (e)	+37 (e)	136 (e)	−0.47
	CsPbI ₃			2.68 (h)	+43 (h)	94 (h)	
				1.35	+21	258	
Schlipf et al. ^[32]	MAPbI ₃	Theoretical	Three-phonon Fröhlich polaron model	1.4	+28		−1.5
Poncé et al. ^[33]	MAPbI ₃	Theoretical	Multi-LO phonon coupling	1.91 (e)		33 (e)	−1.37
				1.75 (h)		50 (h)	
	CsPbI ₃			1.69 (e)		76 (e)	−0.92
				1.63 (h)		61 (h)	
	CsPbBr ₃			2.36 (e)		41 (e)	
				2.15 (h)		44 (h)	
	CsSnI ₃			0.75 (e)		177 (e)	
				0.97 (h)		241 (h)	
CsSnBr ₃	1.20 (e)		89 (e)				
	1.63 (h)		61 (h)				
Sender et al. ^[22]	MAPbI ₃	Experimental	Far-IR spectroscopy, then using single-phonon Fröhlich model	1.72	+35	197	
	MAPbBr ₃			1.69	+35	158	
	MAPbCl ₃			2.17	+48	58	
Zhao et al. ^[69]	MAPbBr ₃	Experimental	THz spectroscopy, then using single-phonon Fröhlich model	1.68 (e)		83 (e)	
				1.17 (h)		265 (h)	
Lan et al. ^[70]	MAPbI ₃	Experimental	THz spectroscopy, then using single-phonon Fröhlich model	2			
Batignani et al. ^[108]	MAPbBr ₃	Experimental	Raman spectroscopy, then using single-phonon Fröhlich model	1.84 (e)			
				1.28 (h)			
Puppin et al. ^[196]	CsPbBr ₃	Experimental	ARPES direct measurement of m^* , then using single-phonon Fröhlich model	1.82 (h)	+50 (h)		
Neutzner et al. ^[84]	(PEA) ₂ PbI ₄	Experimental	Temperature-dependent PL line-width measurements, then using single-phonon Fröhlich model	1.67 – 2.2			
Manna et al. ^[152]	Cs ₂ AgBiCl ₆	Theoretical	Single-phonon Fröhlich model	2.82 (e)	+67 (e)	17 (e)	
				3.35 (h)	+84 (h)	9 (h)	
	Cs ₂ AgIn _{0.25} Bi _{0.75} Cl ₆			2.41 (e)	+55 (e)	30 (e)	
				3.02 (h)	+73 (h)	14 (h)	
				3.93 (e)	+104 (e)	5 (e)	
	Cs ₂ AgIn _{0.75} Bi _{0.25} Cl ₆			3.15 (h)	+77 (h)	10 (h)	
				1.99 (e)	+43 (e)	52 (e)	
4.66 (h)	+132 (h)	2 (h)					
Steele et al. ^[148]	Cs ₂ AgBiBr ₆	Theoretical	Single-phonon Fröhlich model	2.54 (e)			
				2.0 (h)			

We distinguish between theoretical and experimental studies, and give a brief description of the approach used to calculate the parameters. We use the term “single-phonon Fröhlich model” for the expression for α_F given in the main text, based on the high-frequency and static dielectric constants ϵ_∞ , ϵ_{static} , and the extracted LO-phonon frequency ω_{LO} .

more detail in a variety of materials,^[54,55] notably by Williams and Song,^[34,56] and is associated with instances of strong localization. Cases of self-trapping can be purely intrinsic, where the formation of a self-trapped state automatically leads to a lower-energy configuration, or can be extrinsic, where an already-present lattice defect leads to charge localization, which induces a further lattice distortion at that site.^[8] In some cases, self-trapped charges recombine radiatively with a free charge, at so-called “color centers”.^[57,58] Both color centers and strongly self-trapped charges are often described as a “molecule in a crystal,” that is, the formation of a covalent bond in an ionic crystal, because their energy levels resemble those of halogen molecule negative ions X_2^- .^[55,57–59] Although the terminology varies, all of these states involve the formation of a polaron and lead to a qualitative change in the properties associated with charges, such as their effective mass, mobility or energetics.^[15–18,25,60]

2.3. Emin and Holstein’s Evaluation of Polaronic Regimes

A useful framework for considering the large and small polaron regimes was outlined by Emin and Holstein,^[61] and summarized by Stoneham et al.^[58] One can consider four contributions to the energy of an electron coupling to a polarizable lattice, via short- and long-range interactions, and coupling to a defect state. These contributions depend on the electronic wavefunction length scale L , with $L = 0$ corresponding to an infinitesimally localized state at a lattice site. The kinetic energy of the charge carrier scales as $+L^{-2}$. The short-range interaction scales as $-L^{-d}$ (where d is the number of dimensions of the system); the long-range interaction scales as $-L^{-4-d}$; and a cross-term from the short- and long-range interactions scales as $-L^{-2}$. Finally, the defect potential is assumed to be Coulombic, and thus scales as $-L^{-1}$. Overall, using the same notation as Emin and Holstein, the total energy may be expressed as:

$$E(L) = \frac{T_e}{L^2} - \frac{1}{2} \left(\frac{V_{int}^s}{L^d} + \frac{V_{int}^l}{L^{4-d}} + \frac{V_{int}^{s,l}}{L^2} \right) - \frac{V_d}{L} \quad (2)$$

where T_e , V_d and $V_{int}^{s,l}$ are constants associated with the kinetic energy, defect potential, and the charge–lattice interactions, respectively, and d is the number of dimensions of the system. For a 3D system, the expression is thus:

$$E(L) = \frac{T_e}{L^2} - \frac{1}{2} \left(\frac{V_{int}^s}{L^3} + \frac{V_{int}^l}{L} + \frac{V_{int}^{s,l}}{L^2} \right) - \frac{V_d}{L} \quad (3)$$

In the 3D case, four distinct situations can arise, which are sketched out in **Figure 1**. If the charge–lattice interaction is purely long-range a single minimum exists in the dependence of energy on L , giving only large polarons that are stably bound (Figure 1a), and this situation is qualitatively the same whether or not a defect potential is present. In cases with only short-range interactions, the energy has a minimum at $L = 0$, giving a small polaron, and at $L = \infty$, giving a free charge (Figure 1b). In the presence of both a defect potential and a short-range charge–lattice coupling, a small polaron state can always form at $L = 0$, and the large polaron state at finite L can be metastable (Figure 1c) or unstable (Figure 1d).

2.4. The Role of Dimensionality in Charge-Carrier Localization

There have been suggestions that the formation of small polarons depends on the dimensionality of the system:^[56,61,62] 2D and 3D systems may have an energetic barrier between free and localized states (as shown schematically in Figure 1b for small polarons), whereas this barrier has been argued to be effectively zero in 1D systems.^[63] Such effects are evident from Equation 2: in one or two dimensions the exponent of interaction terms will be different,^[61] altering the dependence of energy on L and removing the barrier between the free electron and small polaron states displayed in Figure 1b. Experiments have provided some confirmation of this dependence, with 3D RbI showing self-trapped state formation over a few nanoseconds,^[64] whereas 1D systems display much faster small polaron formation,^[65,66] on picosecond timescales, implying the presence of low to no energetic barriers.

2.5. Applying Polaron Theory to Metal-Halide Semiconductors

Both the Fröhlich and Holstein Hamiltonians are simplified models, and there are inherent difficulties in calculating polaronic effects, especially long-range interactions, when computational methods are based on small systems that often cover only a handful of unit cells.^[49,67,68] However, they provide useful frameworks within which to discuss interactions between charges and phonons, and can be expanded upon and adapted to specific cases, as discussed below.

Approaches to describe large and small polarons have been attempted across a variety of metal-halide semiconductors, with varying degrees of success. Theoretical descriptions of polarons in typical bulk 3D metal-halide perovskites (used to describe materials with formula ABX_3 such as $MAPbI_3$, shown in **Figure 2a**) have focused on Fröhlich-type couplings, and these have been developed with constant input from experimental results across the field.^[21,22,50,53] As we discuss below, calculations of the Fröhlich coupling parameter α_F have yielded values between 1 and 2 for bulk 3D lead-halide perovskites,^[22,69,70] comfortably within the weaker coupling regime of large polarons. Theoretical descriptions of less investigated metal-halide semiconductors, such as double perovskites or low-dimensional metal-halides, are more difficult because of their more heavily disordered crystal structures,^[7,12] although attempts have been made to describe how small polarons and self trapping can lead to emission in layered Ruddlesden–Popper perovskites,^[71–73] and calculations of the influence of lattice anharmonicity on Feynman/Hellwarth polarons in vacancy-ordered perovskites have also been carried out.^[74,75] Further, there have been suggestions that it is the electronic dimensionality of a material (described as the connectivity between the orbitals that make up the conduction band minimum and valence band maximum),^[76] as opposed to its structural dimensionality, that is the more important feature in determining suitability for different optoelectronic applications.^[76,77] Thus, materials with a high electronic dimensionality are more likely to have lower charge-carrier effective masses, isotropic charge-carrier transport and shallower defect states,^[76] making them ideally suited for solar cell devices, whereas the converse case of low electronic dimensionality might be more applicable to broadband, white-light emitting diodes.^[77]

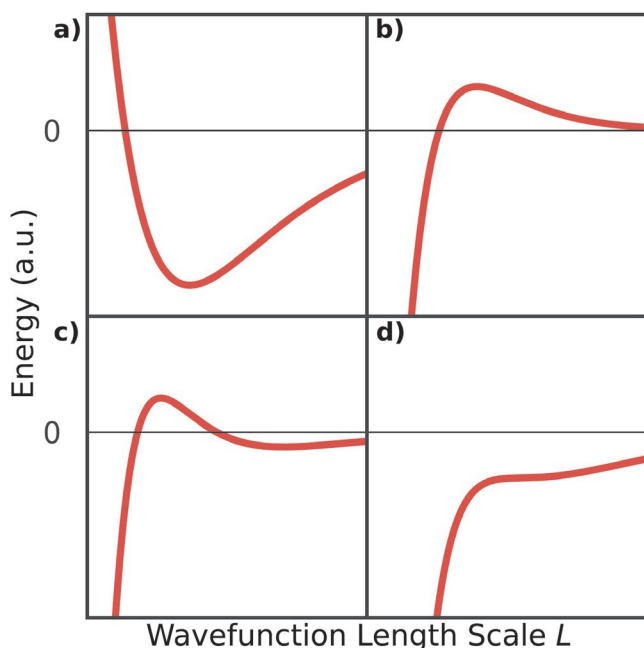


Figure 1. Schematic plots of energy against length scale L of the electronic wavefunction, adapted from Emin et al.^[61] The figures describe the energy of a polaron in a 3D polar material where a charge can interact with the potential of a defect, and with the lattice via long- and short-range interactions, as described in the main text. In case (a), the charge interacts only with the lattice via a long-range interaction, leading to a stably bound large polaron forming at finite L . When the charge interacts only with the lattice through a short-range potential, a small polaron can form at $L = 0$ or charge carriers are free as L tends toward infinity, as in case (b). When the charge interacts with a defect potential and with the lattice via a short-range potential, a small polaron will always form at $L = 0$, and the large polaron state is metastable, as in (c), or unstable, as in (d). Adapted with permission.^[61] Copyright 1976, American Physical Society.

3. Experimental Approaches for Observing Polaronic Effects

To facilitate the discussion of polaronic effects across different classes of metal-halide semiconductors, we have included some of the most common structures adopted by metal-halide semiconductors in Figure 2. Such materials include bulk 3D MHPs with chemical formula ABX_3 , double perovskites with chemical formula $A_2B'B''X_6$, Ruddlesden–Popper perovskites with composition $R_2A_{n-1}B_nX_{3n+1}$ (R is a longer organic cation, relative to the small A-site cation, and n is the number of octahedral planes), two types of vacancy-ordered perovskites with compositions $A_2\Box B^4X_6$ and $A_3\Box B_2^3X_9$ (\Box indicates a vacancy), and two types of quasi-0D metal halides with $[MX_6]$ octahedra and $[MX_5]$ pyramids. For these materials, a variety of experimental techniques have been implemented in order to explore charge-carrier localization and polaronic effects, as discussed below.

3.1. Steady-State Photoluminescence and Absorption

Measurements of a semiconductor's photoluminescence and absorption spectra provide insights into its energetic distribution of states,^[78] although steady-state optical absorption cannot

provide direct evidence of polaronic states as polaron binding energies tend to be in the infrared (IR) (discussed below).

In the case of weak charge-carrier localization, such as in $MAPbI_3$, the effects of large polaron formation on steady-state absorption and photoluminescence (PL) are relatively small, and the influence of electron–phonon couplings on PL linewidths have mainly been investigated via temperature-dependent measurements, as discussed below. Modeling such phenomena accurately from first principles is difficult, and requires a summation over all phase space available for charge-carrier scattering events within the band structure of a semiconductor, which has, for example, been done through GW first-principles calculations for hybrid lead halide perovskites.^[79] Such calculations depend on similar factors to those entering the Fröhlich parameter α_F , such as the dielectric constants, Born effective charges and vibrational frequencies; however, because of the complexity of such calculations they may not be directly relatable to α_F through a simple analytical expression.

In the case of strong localization radiative recombination typically displays highly Stokes-shifted emission, several hundred meV lower than absorption energies, because large energetic losses are associated with the induced lattice deformation and with changes in the kinetic and potential energy of the charge carrier.^[6,56,80] Both very strong electron–phonon coupling to a single state, or the presence of multiple self-trapped states within a material, can lead to broadband white-light emission, as has been observed in several Ruddlesden–Popper perovskites and the metal-halide material $Rb_4Ag_2BiBr_9$.^[8,35,81] In the case of stronger couplings, spectra can sometimes be well-captured by the Huang–Rhys oscillator model,^[82] which is a simplified model based on the Frank–Condon principle for optical transitions, with the spectra composed of electronic transition replica separated by an associated phonon energy E_{ph} . Although this model is not applicable in all cases,^[82,83] it has been used successfully to model the PL spectra of the double perovskite $Cs_2AgBiBr_6$ (shown in Figure 3a),^[11] and to describe the low-temperature absorption spectra of Ruddlesden–Popper perovskites.^[84]

We also note that it is important to distinguish the red-shifted PL arising from strongly localized states from that originating instead from sub-gap electronic trap states. It has recently been suggested that excitation with photons of energy falling below the bandgap may be one way to distinguish polaronic from trap-state emission, given that some sub-gap trap states may be directly excitable, while polaron formation generally requires excitation with above-gap photon energies. Since a PL emission band was present for both above- and below-bandgap excitation, Kahmann et al. ascribed emission from Ruddlesden–Popper perovskites to deep defect states, as opposed to the formation of self-trapped excitons.^[85]

Measurements of Urbach energies, from fits of the exponential tail of optical absorption, are sometimes used as a proxy for quantifying the strength of electron–phonon coupling in a material,^[86] although such low-energy tails can often simply reflect the amount of energetic disorder in a material without providing fundamental insights,^[78,87] and we would caution against using them as a measure of charge-carrier localization. There is also significant uncertainty around interpretations of the fluence dependence of the intensity of measured photoluminescence

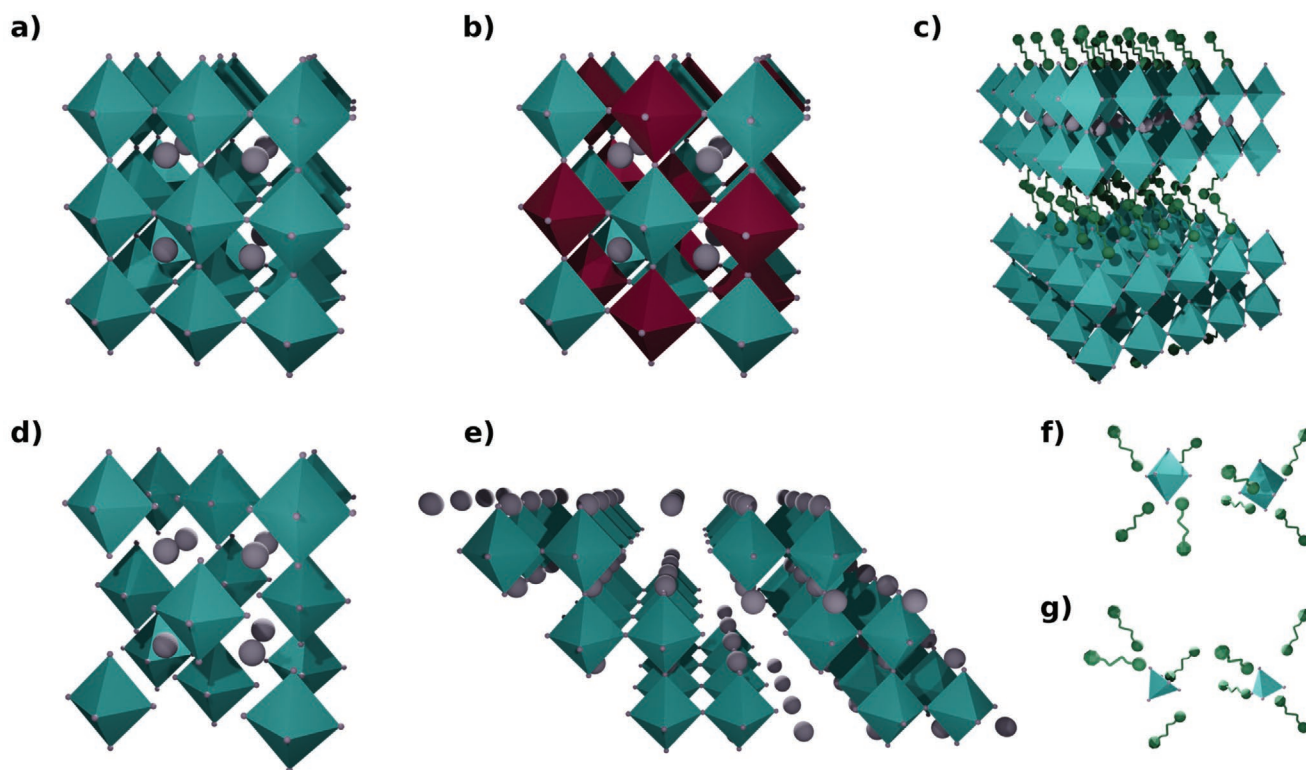


Figure 2. Example structures for some of the material classes discussed here. a) Bulk 3D perovskites with composition ABX_3 , with characteristic corner-sharing octahedra for which the halide ions are located at the octahedral corners and the metal ions are located in the center of the octahedra. The A-site cation is located at the center between octahedra. b) Double perovskites, for which alternating metal ions are located at the center of adjacent octahedra (shown by different colours). c) An $n = 2$ Ruddlesden–Popper perovskite, for which the larger organic cations (in green) separate planes of corner-sharing octahedra. d) 2–1–6 Vacancy-ordered perovskites, where metal ions have been removed from alternating sites in a chequered pattern. e) 3–2–9 Vacancy-ordered perovskites, for which every third metal ion has been removed along the $\langle 111 \rangle$ directions. f, g) Finally, two different types of quasi-0D metal-halides, with $[MX_6]$ octahedra (f) and $[MX_5]$ pyramids (g).

spectra, given the difficulty of establishing a variety of parameters: whether the photoexcitation is pulsed or continuous-wave; whether the emission arises from a localized state, excitons or band-to-band recombination; whether the emission is measured using time-resolved spectroscopy or in steady-state conditions; and whether the density of photoexcited charge-carriers leads to monomolecular, bimolecular or Auger recombination dominating.^[4,78,88] Thus, again we would caution against over-interpretation of such measurements to prove or disprove the presence of polaronic effects, especially if such analysis is not supported by other experimental techniques.

3.2. Temperature-Dependent Photoluminescence

Temperature-dependent photoluminescence measurements are crucial for an examination of the activation of phonon modes and the influence of phonon interactions on the broadening of PL spectra. Electron–phonon couplings can depend on the phonon occupancy of states, which is given by the Bose–Einstein distribution.^[78,89] In the case of acoustic phonons, whose energy is much smaller than $k_B T$ over typical experimental regimes, this dependence is approximated as linear, allowing the contribution from acoustic deformation potential couplings to be distinguished from that of Fröhlich-type couplings to LO

phonons.^[78,79,89] Wright et al. used measurements of PL broadening to extract LO phonon energies and electron–phonon coupling constants for 3D MHPs, showing that Fröhlich couplings were the dominant source of PL broadening.^[79] Similarly, PL arising from localized states typically narrows and increases substantially in intensity as temperature is lowered,^[34] a behavior that has been observed across a range of materials including MHPs,^[79,90] Ruddlesden–Popper perovskites,^[91] OD tin-halides,^[12] vacancy-ordered perovskites,^[10] and the metal-halide $Rb_4Ag_2BiBr_9$, (see Figure 3b).^[81] Further, in the case of small polarons or self-trapped charges, the lifetime of PL increases substantially, as measured by time-resolved PL spectroscopy, because charges cannot de-localize as easily and other non-radiative recombination pathways become less effective.^[12,34,92] Given that photoluminescence spectra can have multiple contributing processes, variation of temperature can help further distinguish between band-to-band recombination, emissive trap states and self-trapped emission,^[91] or between emission from self-trapped states occurring at particular lattice sites.^[81]

3.3. Temperature-Dependent Charge-Carrier Mobility

Polaronic effects fundamentally alter the way charge carriers move within a lattice, meaning that temperature-dependent

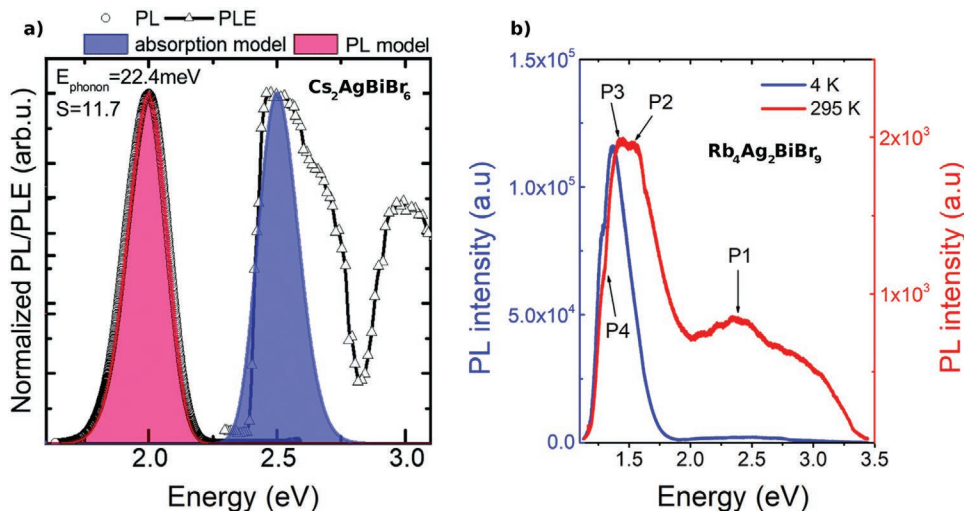


Figure 3. Characteristic behavior of photoluminescence that arises from strongly localized charges, notably exhibiting large Stokes shifts, broadband emission and significantly increased PL intensity at lower temperatures. a) Photoluminescence and photoluminescence excitation spectra, with their respective Huang–Rhys model fits, for $\text{Cs}_2\text{AgBiBr}_6$.^[11] The large phonon energy, high Huang–Rhys parameter value and large Stokes shift, as well as Raman measurements, led Zelewski et al.^[11] to attribute the emission at 2 eV to a color center. Reproduced with permission.^[11] Copyright 2019, The Royal Society of Chemistry. b) Photoluminescence spectra of $\text{Rb}_4\text{Ag}_2\text{BiBr}_9$ at 4 and 295 K, with four separate emission peaks P1–P4 identified.^[81] The sharp increase in emission intensity of peaks P2–P4 as temperature decreases is part of the evidence used to argue that emission bands arise from distinct self-trapped states located on $[\text{BiBr}_6]$ structural units.^[81] Reproduced with permission.^[81] Copyright 2019, American Chemical Society.

measurements of their mobility give insights into the nature of different scattering processes that affect their motion. Within the conventional Drude model, charge-carrier mobilities depend on both scattering rates and effective masses as $\mu = \frac{q\tau}{m^*}$, where τ is the momentum relaxation time (which can have multiple contributions). Although this simplified model does not necessarily capture effects of charge-carrier localization particularly well, it can be illustrative of its effects: when large or small polarons form, increases in m^* or changes in electron–phonon scattering will alter charge-carrier mobilities.^[3,32] As temperature is varied, polaron formation and transport dynamics change (for example, via the scaling of temperature with respect to LO phonon energies), and the dominance of different mechanisms yields different dependencies for $\mu \propto T^p$. In the case of Fröhlich-type couplings, the mobility increases with falling temperature, as the LO phonon mode contribution decreases,^[47,51,78] behavior which is typically found in 3D bulk MHPs.^[3,21,32] In contrast, the temperature-activated hopping that is typical of small polarons leads to mobilities increasing with higher temperature.^[17,93] Measurements of temperature-dependent charge-carrier mobilities using optical-pump, terahertz-probe (OPTP) spectroscopy and time-resolved microwave conductivity (TRMC) have yielded insights across a variety of materials, with MAPbI_3 ,^[94] MAPbBr_3 ,^[95] FASnI_3 ,^[96] and the double perovskite $\text{Cs}_2\text{AgBiBr}_6$ ^[97] having been reported to show exponents around $p \approx -1$ to -1.5 . However, less negative exponents have also been reported, as for example for FAPbI_3 ($\mu \propto T^p$ with $p \approx -0.53$)^[98] and for the low-temperature tetragonal phase of MAPbBr_3 ($p \approx -0.5$).^[95] However, it is important to note that a variety of both intrinsic and extrinsic factors will contribute to the exact value of p encountered in a material, as has been discussed extensively in other reviews.^[3,50]

While p may be influenced by the intrinsic electronic coupling to a variety of phonon modes,^[33] extrinsic factors such as scattering off grain boundaries or ionic impurities will also impart a strong temperature dependence on the charge-carrier mobility.^[50,96]

3.4. Far Infrared and Vibrational Spectroscopy

Far IR and vibrational spectroscopy are able to probe energy scales ranging from tens to hundreds of meV, providing direct insights into the phonon modes that charge carriers couple to in metal-halide semiconductors and enabling direct measurements of the binding energies typically associated with large and small polarons in these materials.^[80] Pérez-Osorio et al. conducted a wide-ranging study of the IR vibrational properties of thin-film MAPbI_3 , combining a variety of IR absorption measurements and theoretical calculations to show significant low-energy ($< 110\text{ cm}^{-1}$, 14 meV) contributions from LO phonons to the static dielectric constant.^[99] Assuming that effective masses m^* of charge carriers are known, then one can use optical phonon frequencies and dielectric constants measured using IR spectroscopy to calculate the Fröhlich coupling parameter α_F , following Feynman and Hellwarth’s approaches.^[18,45] Sendner et al. used this method to calculate the polaron effective mass, binding energy and mobility in different lead-halide perovskites (see Figure 4).^[22] Excited-state IR spectroscopy that probes the IR absorption spectrum following optical photoexcitation of charge carriers can also be used to measure the dynamics and energetics of polaron states;^[100] combining these measurements with theoretical descriptions of polaron absorption bands can provide valuable insights into polaron binding

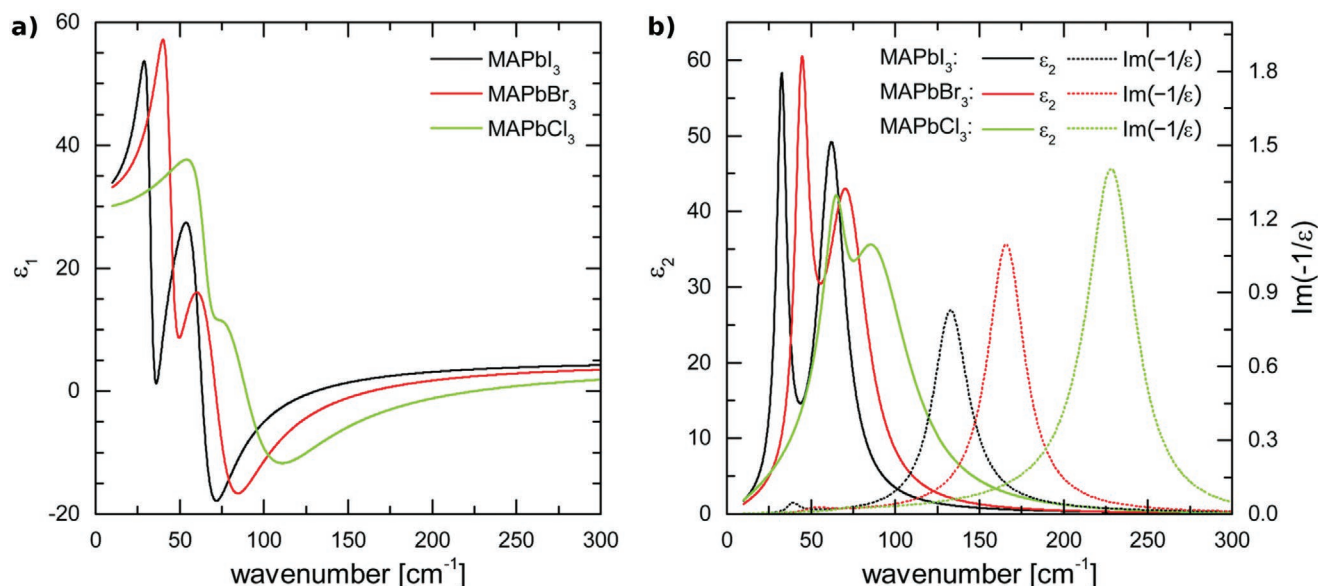


Figure 4. Dielectric function in the far IR range for MAPb(Cl/Br/I)₃, calculated from transmittance measurements by Sendner et al.^[22] a) Real part of the dielectric function ϵ_1 in solid lines. b) Imaginary part of the dielectric function ϵ_2 in solid lines, and the loss function $\text{Im}[-1/\epsilon(\omega)]$ in dashed lines. Peaks in ϵ_2 correspond to transverse optical phonons, and peaks in the loss function correspond to longitudinal optical phonons. The frequencies of the phonons can be used to calculate the value of ϵ_{static} , and then also the Fröhlich coupling parameter α_f and polaron mass.^[22,43,44] a, b) Reproduced under the terms of the CC-BY Creative Commons Attribution 3.0 Unported license (<https://creativecommons.org/licenses/by/3.0>).^[22] Copyright 2016, The Royal Society of Chemistry.

energies and the extent of charge-carrier localization.^[51,80] Raman spectroscopy has also enabled measurement of phonon frequencies and quantification of electron–phonon scattering in the double perovskite Cs₂AgBiBr₆,^[11] vacancy-ordered metal-halides,^[10] and 2D lead halide perovskites.^[101]

3.5. Ultrafast Spectroscopy

Given that polaron formation often occurs on picosecond timescales, ultrafast spectroscopy can provide a window into the transient dynamics of charge carriers as they localize. OPTP measurements can give insights into both ultrafast dynamics and charge–lattice couplings,^[102–105] whilst Transient Absorption (TA) experiments can probe dynamics associated with a variety of optical transitions, which can be affected by polaronic processes, as shown in **Figure 5**.^[8,101,106,107] Ultrafast spectroscopy in the IR region provides information on the dynamics of specific phonon modes and polaron formation dynamics,^[100,108] as demonstrated recently by Munson et al. in their study of polaron formation in (MA/FA/Cs)PbBr₃.^[109] Alternative spectroscopic approaches have included optical Kerr effect spectroscopy and 2D spectroscopy,^[84,110,111] both of which are also able to provide sub-picosecond time resolution, as well as slower techniques such as X-ray transient absorption, which can give insights into structural distortions in a material.^[112–114] We would caution that, although these techniques can provide valuable information regarding ultrafast processes in metal-halide semiconductors, in general there can be a variety of contributing signals at early times and great care needs to be applied when interpreting specific transient experimental signals.

3.6. Experiments Under High Magnetic Fields

The presence of strongly bound polarons can be probed using magnetic fields, the presence of which modifies the measured optical absorption spectrum of the polarons.^[49,115] For example, polarons are expected to exhibit a cyclotron resonance at a frequency $\omega_c = qB/m_p$, where m_p is simply the polaron effective mass and B is the magnetic field,^[49] and early experiments on silver halides confirmed the potential of such studies for determining polaron effective masses.^[116] More recent spectroscopy under high magnetic fields has focused on determination of effective masses and binding energies of excitons, and their coupling to phonons, in bulk 3D and layered Ruddlesden–Popper perovskites.^[117–121] For example, one very recent study reported magneto-optical absorption measurements of $n = 1–6$ layered Ruddlesden–Popper perovskites, demonstrating how carrier effective masses may be tuned by varying the number of octahedral layers or swapping lead for tin at the B-site cation.^[122] Comparison of such experimentally determined masses with those derived from band structure calculations, made without consideration of polaronic effects, may further elucidate the extent to which polaronic contributions enhance carrier masses in reality.

4. Polarons in Metal-Halide Semiconductors

4.1. Bulk 3D Metal-Halide Perovskites

The nature and impact of polarons in bulk 3D metal-halide perovskites (such as MAPbI₃ or FASnI₃, FA = CH(NH₂)₂, see Figure 2a) has undergone significant debate, with both theoretical and experimental contributions seeking to clarify

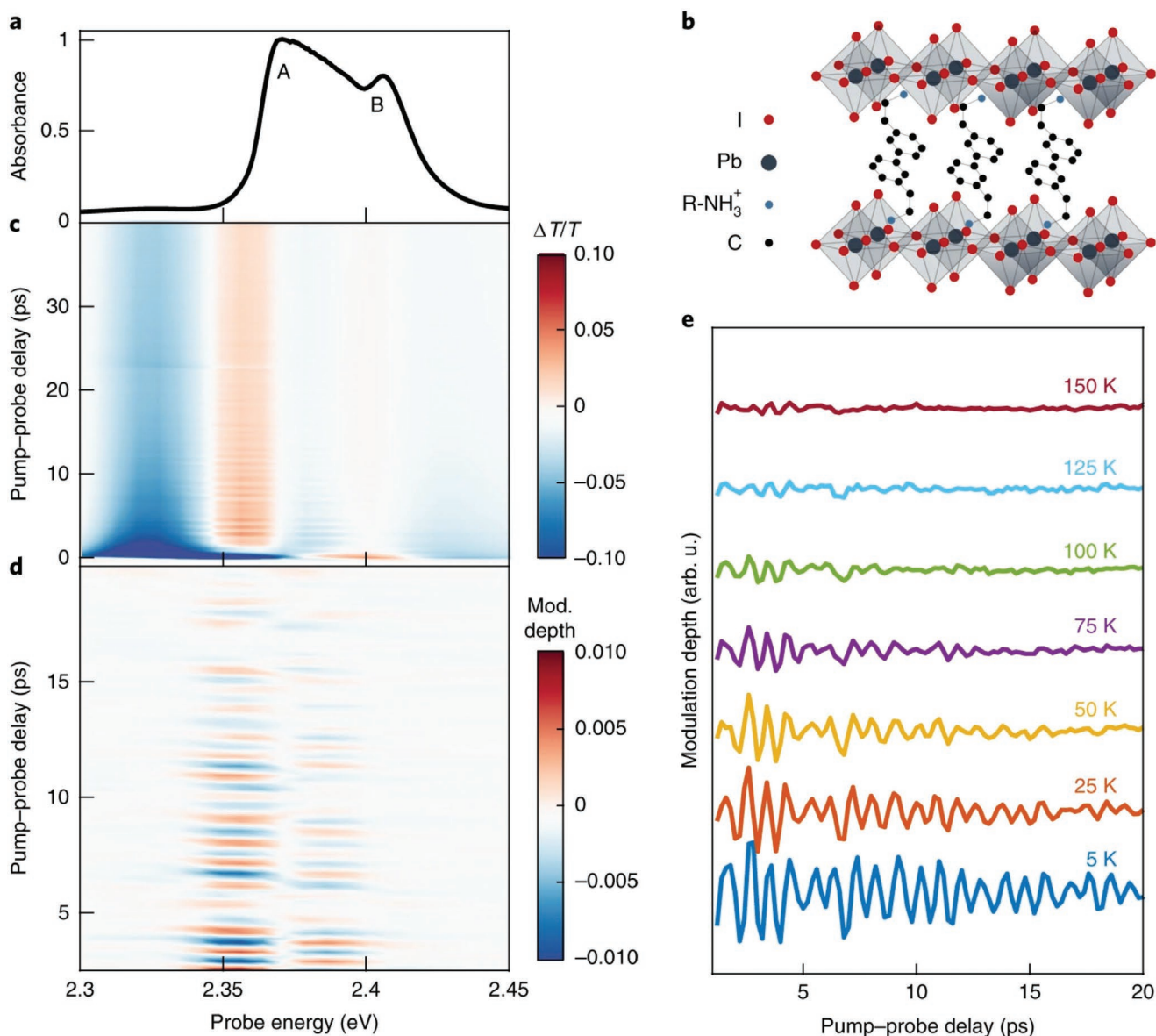


Figure 5. Measurements of $(\text{PEA})_2\text{PbI}_4$ by Thouin et al.^[101] based around ultrafast transient absorption. a) Exciton absorption spectrum measured at 5 K. b) Schematic of crystal structure of $(\text{PEA})_2\text{PbI}_4$. c) Time-resolved differential transmission $\Delta T/T$, measured at 5 K with a pump energy of 3.06 eV. d) Oscillatory components from (c), obtained by subtracting the population dynamics. e) Temperature dependence of the oscillatory response, taken from slices at 2.35 eV. The oscillations are short-lived and weak at 150 K, mainly because of dynamic disorder.^[101] As temperature decreases, clear coherent oscillations on a picosecond timescale are visible due to phonon modulations. The Fourier transform of the oscillations shows the presence of six low-energy ($<50 \text{ cm}^{-1}$) phonon modes, which match well with the calculated phonon modes, and which contribute to the formation of electron and hole polarons in $(\text{PEA})_2\text{PbI}_4$.^[101] a–e) Reproduced with permission.^[101] Copyright 2019, The Authors, published by Springer Nature.

our understanding of MHPs.^[6,23,25,50] Whereas scattering in the classic inorganic semiconductor silicon is dominated by couplings to acoustic phonon modes,^[78] as it is a non-polar material, MHPs are ionic materials with a highly polarizable lattice that leads to much stronger interactions between charge carriers and longitudinal optical phonon modes, more similar to the case of the polar semiconductor GaAs.^[21,32,50] As such, there was some initial discussion around whether charge-carrier interactions with the lattice in 3D bulk MHPs were dominated by acoustic deformation potential scattering,^[13,123]

but these approaches struggled to accurately replicate measured charge-carrier mobilities or their temperature dependence. Instead, there is now broad acceptance that interactions are dominated by Fröhlich-type interactions of charge carriers with the electric fields generated by LO phonons of the polar ionic sub-lattice.^[21,32,79] Frost applied the Fröhlich/Feynman polaron model to MHPs, and although the results produced good qualitative agreement with experimental results, they failed to replicate the experimentally observed $T^{-1.5}$ temperature dependence for the charge-carrier mobility.^[21] More recently,

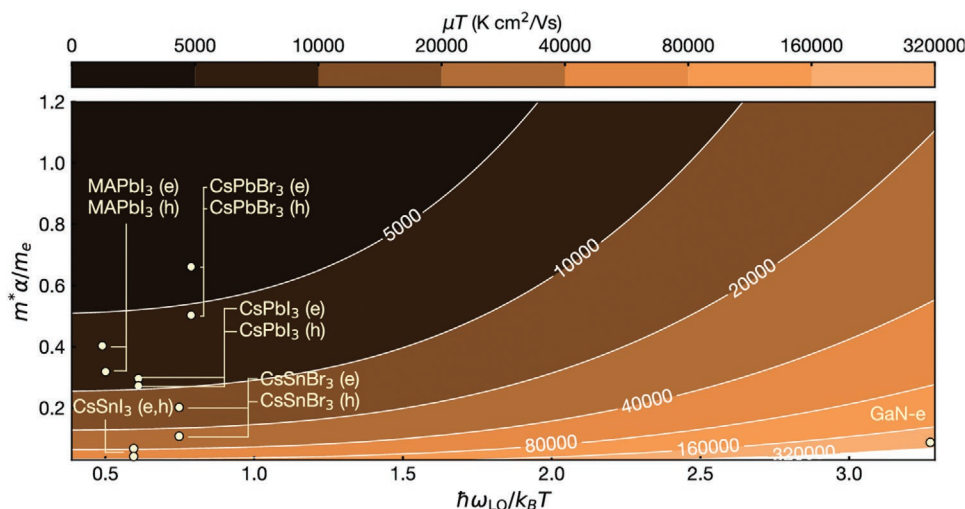


Figure 6. Figure taken from Poncé et al.^[33] showing the dependence of charge-carrier mobility on Fröhlich coupling strength α_F , band effective mass m^* and LO phonon frequency ω_{LO} for a variety of semiconducting materials, calculated using a model that includes Fröhlich-type electron–phonon coupling. In this model, the mobility only depends on two dimensionless parameters: $\alpha_F m^* / m_e$, referred to as the “polar mass,” and the ratio of LO phonon and thermal energies, $\frac{\hbar\omega_{LO}}{k_B T}$. The x-axis values are calculated for $T = 300$ K ($k_B T = 25.9$ meV), and the labels e, h correspond to electron and hole mobilities, respectively. Materials with higher LO-phonon frequencies or smaller “polar masses,” at a given fixed temperature, have higher charge-carrier mobilities. Reproduced with permission.^[33] Copyright 2019, American Chemical Society.

attempts have been made to expand upon the simplified Fröhlich model by extending the coupling to three distinct groups of LO phonons,^[32,33] or by developing new ab initio theories that encompass both Fröhlich polar couplings and non-Fröhlich couplings to acoustic and optical phonons:^[60,68] both approaches appear to replicate measured trends in charge-carrier mobility with temperature better than previous attempts.

4.1.1. Fröhlich Coupling Strengths and Phonon Anharmonicity

Various attempts at quantifying the polaron coupling strength α_F in MAPbI₃ have been made,^[21,22,33] and we provide a summary of values across a range of MHPs in Table 1. Values tend to lie in the range of $\alpha_F = 1$ –2, with renormalization of carrier effective masses limited to between 20% and 50% of the band effective mass, indicating that polaronic effects in MHPs are limited to the weak-to-intermediate coupling range, that is, behavior that is well described by Fröhlich-type large polarons. These couplings do serve to limit charge-carrier mobilities at room temperature, with the effect varying between different halide and metal anions,^[3] as discussed below and as can be seen in **Figure 6**. Further, Munson et al. carried out mid-IR measurements on MAPbI₃, from which they calculated a polaron delocalization length of 9–13 nm,^[100] much larger than the unit cell lengths on the order of approximately 1 nm for tetragonal MAPbI₃,^[124,125] clearly placing polarons in this material in the “large” regime.

There has been discussion around the suitability of the simple Fröhlich model to bulk 3D MHPs, given that it is based upon a harmonic approximation for lattice potentials,^[24,33] with some arguing that lattice anharmonicity plays a more substantial role in soft 3D bulk MHPs than in most polar inorganic semiconductors.^[52,126,127] A recent study by Mayers et al.^[53]

applied a molecular dynamics approach to account for large-scale, low-frequency anharmonic lattice motion; this approach replicated the temperature dependence of both the charge-carrier mobility and bandgap in MAPbI₃ reasonably well.^[53]

4.1.2. The Influence of Compositional Variation on Electron–Phonon Coupling in MHPs

Compositional variation does allow for some tuning of electron–phonon interactions in 3D bulk MHPs. Both computational and experimental studies show that replacing iodine with bromine at the X-site leads to stronger polaronic couplings,^[79,128] and MAPbI₃ and MAPbBr₃ exhibit different temperature dependence of charge-carrier mobilities,^[94,98] potentially indicating further variations in electron–phonon couplings in each material. Wright et al. investigated the temperature-dependent photoluminescence of (MA/FA)Pb(I/Br)₃ to obtain LO phonon energies of $\hbar\omega_{LO} = 11.5, 15.3$ meV and LO phonon coupling strengths of $\gamma_{LO} = 40, 60$ meV in the iodide and bromide MHPs, respectively.^[79] (They also provided a very informative list of phonon coupling strengths across a wide range of inorganic semiconductors in their Supporting Information.) Further, Sendner et al. used far-IR measurements on MAPb(I/Br/Cl)₃ to derive polaron effective masses and electron–phonon coupling constants for each material, placing upper limits on the charge-carrier mobility in single-crystal MAPb(I/Br/Cl)₃ of $\mu \approx 200, 160, 60$ cm² V^{−1} s^{−1} respectively.^[22] As outlined in Equation 1, the Fröhlich coupling strength depends on the inverse of the effective dielectric constant of the material, defined as $\frac{1}{\epsilon_{\text{eff}}} = \frac{1}{\epsilon_{\infty}} - \frac{1}{\epsilon_{\text{static}}}$. Given that lead-bromide MHPs have more ionic metal-halide bonds, leading to a lower value for ϵ_{eff} , the observed stronger couplings can be

easily explained within the Fröhlich polaron picture.^[79] This effect is also apparent from calculations carried out by Poncé et al. for charge-carrier mobilities in MHPs, shown in Figure 6, which reveal that stronger lattice couplings for bromide MHPs lead to a larger “polaronic mass” and thus lower charge-carrier mobilities.^[33]

There has been significant debate around the role of the A-site cation,^[25] notably on whether the replacement of dipolar organic cations (MA/FA) with inorganic Cs may lead to changes in polaron binding energy or formation dynamics.^[128–130] Swapping MA with FA or Cs does not appear to affect ultrafast polaron formation dynamics, although there may be a difference between iodide and bromide MHPs: Bretschneider et al. reported polaron formation times of approximately 400 fs in (FA/MA/Cs)PbI₃,^[104] whereas Munson et al. reported timescales below 150 fs in (FA/MA/Cs)PbBr₃.^[109] Further, mid-IR absorption measurements found no variation in energetics or lattice extent of large polarons when swapping between the three cations,^[109] and temperature-dependent PL also showed little variation in Fröhlich couplings between FA and MA.^[79] Molecular dynamics simulations, combined with Raman measurements, have also been used to argue that replacement of polar MA with Cs does not change the polar, anharmonic fluctuations in lead-halide perovskites.^[52] These findings are in good agreement with the notion that Fröhlich coupling is associated with LO phonon modes of the inorganic metal-halide sublattice in 3D bulk MHPs, with the A-cation having little influence.^[32,99,131]

There have been contradictory claims regarding the effect of replacement of lead with tin at the B-site: Neukirch et al. argue that MASnI₃ has lower polaron binding energies than present in MAPbI₃ for electrons and holes, whereas Mahata et al. argue the opposite and find polaron binding energies to be largest for low Sn content in mixed-cation MAPb_{0.75}Sn_{0.25}I₃. Although replacement of lead with lighter tin indeed leads to higher phonon frequencies,^[132] much of the deterioration in various optoelectronic properties for low tin content can be traced back to higher defect densities and increased non-radiative recombination pathways,^[132,133] without polaronic effects necessarily playing a role. Purely tin-based MHPs have consistently shown higher charge-carrier mobilities than their lead-based counterparts,^[3,96,134] which can be linked to the higher optical phonon frequencies in these materials,^[90,132] as well as the lower effective charge-carrier masses in tin-based MHPs.^[33] Kahmann et al. analyzed the FWHM of PL spectra as a function of temperature for FASnI₃,^[90] following Wright et al.,^[79] and obtained a value of 68 meV for the relevant LO phonon energy, a factor of six higher than that reported for (MA/FA)PbI₃.^[79] However, this seems somewhat too high: an approximate model considering the reduced mass of either Sn–I or Pb–I diatomic chains would predict a factor of approximately 1.1 between the resulting phonon frequencies, and this has indeed been measured for the transverse optical modes in mixed tin-lead iodide perovskites.^[132] In any case, given that the Fröhlich coupling scales as $\alpha_F \propto \omega_{LO}^{-0.5}$, we would expect tin-based MHPs to exhibit lower polaron couplings and higher charge-carrier mobilities compared to their lead-based counterparts—as reported in both theoretical^[33] and experimental work^[3,96,132] (see also Figure 6).

4.2. Perovskite Nanocrystals

The study of perovskite nanocrystals has allowed for comparisons of charge-carrier properties between bulk MHPs and their nanoscale counterparts, with the majority of work focusing on all-inorganic CsPbBr₃ nanocrystals. Early-time photoconductivity studies of CsPbBr₃ nanocrystals, large enough (≈ 30 nm) to be considered as analogues of single crystals, clearly demonstrate the formation of large polarons in this material.^[103] OPTP measurements have also shown that smaller nanocrystals, exhibiting stronger electronic confinement, have broadened, blue-shifted phonon modes that absorb more strongly in the THz frequency domain relative to bulk CsPbBr₃, which is proposed to be caused by a stronger coupling between the THz radiation and optical phonon modes in the nanocrystals.^[135] The broadening of the phonons is associated with shorter phonon lifetimes and is typical of nanoparticles; the blue shift of the modes, however, does not appear to be dependent on size over the studied range (6–10 nm), indicating that phonon confinement is not the sole responsible factor.^[135] These changes in the phonon spectra compared to the bulk perovskite are likely related to structural differences in the lattice, evidenced by XRD studies revealing increasing lattice parameters with decreasing particle size.^[135,136] Such differences in the lattice properties are expected to impact the coupling between phonons and charge carriers, although further studies are needed to confirm and quantify such effects. A study based on TA and molecular dynamics simulations also found strong coupling between charge carriers and phonons in CsPbBr₃ nanocrystals across a range of strong-to-weak confinement (0.8–12 nm).^[137] Further, a study that combined optical and X-ray transient absorption spectroscopy of moderately confined (≈ 8 nm) MAPbBr₃ nanocrystals argued that structural distortions around the Pb²⁺ cation may lead to the formation of small electron polarons.^[113]

Recent work has highlighted the importance of structural distortions in inducing polaron formation across MHPs,^[25,114,138] and a crucial question with regards nanocrystals is whether such structural distortions, and thus polaron formation, are facilitated or inhibited by nanoscale structures, as is the case for quasi-0D metal halides (discussed below). Given that temperature-dependent PL studies have found LO-phonon energies between $\hbar\omega_{LO} = 14$ –33 meV for (FA/Cs)PbBr₃ nanocrystals,^[139–141] similar to the value of 15 meV obtained for bulk FAPbBr₃ by Wright et al.,^[79] as well as a similar LO-phonon couplings (45 meV in nanocrystal FAPbBr₃,^[140] as opposed to 60 meV in bulk^[79]), it is not fully clear how much fundamental change is caused by the formation of nanocrystals. Although polaron formation and electron–phonon interactions are present in MHP nanocrystals, further clarification is needed in order to distinguish the extent to which polaronic behavior is affected by the increased presences of boundaries and surfaces in nanocrystals and the resulting ease of structural distortions, from the effects of electronic confinement that vary with nanocrystal size. Interestingly, intrinsic quantum confinement in nominally bulk FAPbI₃ has recently been shown to be associated with lowered electron–phonon coupling,^[142] suggesting that in the absence of clear material boundaries, such as those present in MHP nanocrystals, electronic confinement may lead to polaronic effects being reduced, rather than enhanced.

4.3. Double Perovskites

By swapping the B-site cation in MHPs with two heterovalent cations of charge 1^+ and 3^+ , double perovskites can be formed with composition $A_2B'B''X_6$, opening up a new class of over 90 000 different materials for investigation (see Figure 2b).^[7,143,144] Given the wide variety of compositions that can be studied, it is difficult to draw any fundamental conclusions with regards the origin of charge–lattice interactions that are valid across all double perovskites. Depending on whether the ions at the B' and B'' sites have lone-pair electronic s^2 states, Zhao et al. separate double perovskites into three classes,^[145] which helps to distinguish these materials based on their electronic dimensionality and thus the likelihood of charge localization occurring.^[77] When both ions contribute lone-pair states (e.g., $\text{Cs}_2\text{InBiCl}_6$), they can be considered as electronically 3D analogous to MAPbI_3 . If only one ion contributes a lone-pair state, then one set of $[\text{BX}_6]$ octahedra is electronically isolated from the other, making these double perovskites electronically quasi-0D, as has been found for $\text{Cs}_2\text{AgBiBr}_6$ and $\text{Cs}_2\text{NaBiCl}_6$.^[144,146] Finally, if neither ion has a lone-pair electronic state, this leads to contrasting contributions to the VBM and CBM,^[145] as is the case in $\text{Cs}_2\text{AgInCl}_6$ where the electronic character of the VBM is low-dimensional, with quite flat bands and low hole effective masses, whereas the CBM has very curved bands, more typical of 3D bulk MHPs.^[145,147]

Given that lower electronic dimensionality leads to low- or zero-energy barriers between free and self-trapped states,^[61,62] one would expect a higher likelihood of polaron formation in $\text{Cs}_6\text{AgBiBr}_6$ and $\text{Cs}_2\text{AgInCl}_6$, and in other double perovskites electronically analogous to these. Zelewski et al.^[11] combined low-temperature emission, PL excitation and Raman measurements to argue for the presence of a color center as the source of the emission peak at 2 eV in $\text{Cs}_2\text{AgBiBr}_6$ (see Figure 3a), and they were able to successfully replicate the PL and PLE spectra based on a Franck–Condon model with Huang–Rhys factor of $S = 11.7$ and a phonon energy of 22.4 meV (obtained from Raman spectroscopy).^[11] Another study carried out fitting of the temperature-dependent PL linewidth for $\text{Cs}_2\text{AgBiBr}_6$,^[148] obtaining $\hbar\omega_{LO} = 22$ meV, slightly above the equivalent values found for $(\text{FA}/\text{MA})\text{Pb}(\text{I}/\text{Br})_3$,^[79] as well as a much stronger coupling of charge carriers to LO phonons, with a coupling parameter of $\gamma_{LO} = 226$ meV (compared to 40 and 60 meV for FAPbI_3 and FAPbBr_3 , respectively).^[79,148] The stronger coupling of electrons to the LO phonons is also consistent with the lower charge-carrier mobilities measured for $\text{Cs}_2\text{AgBiBr}_6$.^[97]

Studies of $\text{Cs}_2\text{AgInCl}_6$ have shown confinement of holes on $[\text{AgCl}_6]$ octahedra, leading to the formation of self-trapped excitons that result in broadband white-light emission.^[6,149] Strong blue emission, with a large Stokes shift, from antimony-doped $\text{Cs}_2\text{NaInCl}_6$ has also been attributed to self-trapped exciton states,^[150] and calculations of the band structure of $\text{Cs}_2\text{NaInBr}_6$ have been used to argue that small hole-polarons and self-trapped excitons form easily in this material.^[146] Raman measurements of $\text{Cs}_2\text{AgSb}_{1-y}\text{Bi}_y\text{X}_6$ ($X = \text{Br}, \text{Cl}$) nanocrystals indicated very strong charge-phonon interactions that lead to intrinsic self-trapping of charges within a few ps, as measured by ultrafast TA.^[151] Work by Manna et al.^[152] combined Raman measurements with density functional theory (DFT) calculations,

finding Fröhlich coupling constants in the range $\alpha_F = 2\text{--}5$ for $\text{Cs}_2\text{AgIn}_{1-x}\text{Bi}_x\text{Cl}_6$ nanocrystals, and calculations of charge-carrier mobilities using the Feynman/Hellwarth polaron model suggested upper limits of $2\text{--}52$ $\text{cm}^2 \text{V}^{-1} \text{s}^{-1}$ in nanocrystals across the range of x .^[152]

One recent study reported a reduction in the structural dimensionality of the double perovskite $\text{Cs}_2\text{AgBiBr}_6$ into $n = 1, 2$ octahedral layers, analogous to the case of Ruddlesden–Popper perovskites (discussed below).^[153] This work found that reduction of structural dimensionality can modify the electronic band structure of $\text{Cs}_2\text{AgBiBr}_6$, especially in the case of a single octahedral layer, and demonstrated the ease of structural distortion as the number of octahedral layers is reduced, which enhances the likelihood of charge-carrier localization.^[153] Overall, double perovskites appear to show good correlation between their electronic dimensionality and the likelihood of charge localization, making them promising model systems for further experimental studies.

4.4. Ruddlesden–Popper Layered Perovskites

Ruddlesden–Popper perovskites include large organic cations that cannot be incorporated at the A-site,^[9,154] leading to 2D layers of corner-sharing octahedra with a general formula of $\text{R}_2\text{A}_{n-1}\text{B}_n\text{X}_{3n+1}$. An example structure for an $n = 2$ Ruddlesden–Popper perovskite, such as $(\text{PEA})_2(\text{MA})\text{Pb}_2\text{I}_7$ (PEA = phenylethylammonium), is shown in Figure 2c. The variation of type and concentration of the large organic cation allows for close control over the number of connected 2D octahedral planes, and the materials are often referred to by the (hkl) direction in which a 3D MHP lattice has been sliced in order to achieve the layering. As outlined above, polaron formation depends on the dimensionality of the system being studied, and layered Ruddlesden–Popper perovskites appear to be at the threshold for an energetic barrier forming between localized and free states.^[61,62,73,155]

The additional electronic confinement present in Ruddlesden–Popper perovskites, as well as stronger dielectric screening caused by alternating conducting and insulating layers, lead to strong excitonic effects in these materials.^[8,78,156] Indeed, narrow, efficient radiative recombination at low Stokes shift has been observed for several Ruddlesden–Popper perovskites.^[8,9,156] However, in some cases PL from layered perovskites is highly Stokes-shifted, exhibiting a broadband emission spectrum,^[35,91,157,158] typical of emission from self-trapped states.^[56,71] Ultrafast TA and OPTP spectroscopy of the (110) material $(N\text{-MEDA})[\text{PbBr}_4]$ ($N\text{-MEDA} = N^1\text{-methylene-1,2-diammonium}$) showed fast self-trapping of photoexcited carriers, leading to broadband emission from a distribution of self-trapped excitonic states.^[155] Temperature-dependent PL combined with TA and DFT calculations also confirmed the presence of emissive self-trapped small polarons in (100) materials $(\text{EDBE})\text{PbX}_4$ ($X = \text{Br}, \text{Cl}$, and $\text{EDBE} = 2,2\text{-(ethylenedioxy)bis(ethylammonium)}$).^[106] A study of a new cadmium-based single-layer perovskite, $(\text{F}_2\text{CHCH}_2\text{NH}_3)_2\text{Cd}_x\text{Pb}_{1-x}\text{Br}_4$, demonstrated the importance of structural deformation in enabling emission from self-trapped states, with alloyed Cd–Pb materials emitting much more strongly than either purely Cd- or Pb-based

materials because of increased octahedral distortions.^[159] Further, swapping the organic spacer cations between BA to PEA has a significant effect on the intensity and energy of Raman modes^[120] and can alter the charge-carrier effective mass,^[122] thus varying the strength of the electron–phonon interaction. This has been linked to the fact that swapping organic spacer cations modifies the stiffness or “corrugation” of the octahedral layers in Ruddlesden–Popper perovskites, aiding structural distortion and thus impacting on the likelihood of charge-carrier localization in these materials.^[120,122]

Computational studies have tried to describe small polaron formation in single-layer Ruddlesden–Popper perovskites, finding substantial polaron binding energies of several hundred meVs,^[72] as well as strong exciton couplings to Raman modes.^[101] Temperature-dependent TA and time-resolved PL measurements have also been used to argue that phonon couplings in (PEA)₂PbI₄ lead to the formation of electron and hole polarons, and drive transitions between different excitonic states and influence exciton dynamics and diffusion (see Figure 5).^[84,101,160,161] Further, it also appears that variations in exciton binding energies have an effect on the energies of the polaronic state formed in the case of Coulombically bound electron–hole pairs.^[121,162] For example, a recent study has argued that two excitonic states are present in (BA)₂PbI₄ (BA = butylammonium), and that the different binding energies of the two excitons lead to different couplings with the lattice, with a weak exciton binding energy leading to the formation of large polarons.^[162]

We note that there has been some debate around whether closely-spaced features in low-temperature optical absorption spectra of Ruddlesden–Popper perovskites arise from the presence of multiple excitonic states^[84,101,162] or rather from a single excitonic state that couples to a high-energy (≈ 40 meV) phonon mode, leading to vibronic progressions.^[120,163] However, regardless of the origin of these specific features, there is clear literature consensus that the presence of strong electron–phonon couplings to low-energy LO phonon modes of the halide sub-lattice plays a key role in polaron formation in Ruddlesden–Popper perovskites.^[84,101,120,163]

Overall, we find that while several experimental and computational studies have examined the role of polarons in Ruddlesden–Popper perovskites, their role is not yet fully clarified, given that multiple alternate processes have been evoked to explain their absorption and emission features. As highlighted in two recent reviews,^[35,164] many different sources of emission are present in layered perovskites including excitons, lattice defects, light-induced defects, self-trapped states, molecular chromophores in the organic layers, and structural distortions.^[85] Notably, if the emission is not arising from the metal-halide octahedral planes but from the larger organic cations, this immediately rules out polaronic or self-trapped states as the source of photoluminescence. We suggest that for these materials identification of specific localization effects needs to be done with particular care, requiring multiple complementary experimental or theoretical approaches to provide convincing evidence of polaron formation. For example, in certain cases defect states have been found to induce self-trapping (sometimes known as “extrinsic self-trapping”),^[8,56] making it difficult to distinguish emission from an intrinsic self-trapped state to that associated with a radiative trap state;^[35,85] equally, lattice

distortions can both aid the formation of self-trapped states^[58] and alter the electronic properties of layered perovskites,^[85,165] further confusing the impact of structural changes on charge-carrier transport and emission.^[8] Given the wide variety of potential applications for Ruddlesden–Popper perovskites, from solar cells to LEDs,^[9,158] photodetectors or X-ray sensitizers,^[166,167] a better understanding of the fundamental processes governing charge–lattice interactions would be of great value, as has been achieved so far for their 3D analogues. A clearer picture of these couplings would be especially useful with regards to lighting applications, given the interest in achieving efficient, “sun-like” or broadband white-light emission in LEDs.^[37,149,168]

4.5. Non-Perovskite Metal-Halide Semiconductors

Finally, a wide range of non-perovskite metal-halide semiconducting materials have been investigated for potential optoelectronic applications. Some of these research studies date back to original work involving alkali halides and photographic materials,^[34,64,169] with other more recent investigations focusing on MHP-related materials such as vacancy-ordered perovskites.^[10] We focus here on more recent results, and recommend reviews by Stoneham et al.^[58] and by Williams and Song^[34] for comprehensive coverage of earlier work including the alkali halides, vacancies in quartz, and metal-oxides.

4.5.1. Vacancy-Ordered Perovskites

Vacancy-ordered perovskites have been investigated as potential all-inorganic, lead-free variations of MHPs.^[26,170] There are two main types of compositions: materials with the formula $A_3\Box B_2^{3+}X_9$ (\Box indicates a vacancy),^[171] where every third B³⁺ site is unoccupied and the structure involves either quasi-0D dimers of face-sharing octahedra or 2D layers of octahedra (the latter is shown in Figure 2e);^[171] and vacancy-ordered double perovskites with formula $A_2\Box B^{4+}X_6$,^[172] where every other B⁴⁺ site is unoccupied and the structure involves isolated [BX₆] octahedra (shown in Figure 2d).^[26] McCall et al.^[10] combined Raman and temperature-dependent PL measurements to argue that strong electron–phonon couplings in vacancy-ordered $A_3\Box M_2I_9$ (A = Cs, Rb; M = Bi, Sb) gave rise to small polaron formation, with broad, highly Stokes-shifted emission arising from self-trapped excitons.^[10] Another study combined optical and x-ray transient absorption with DFT calculations to argue for the formation of small polarons in $Cs_3\Box Bi_2Br_9$, through the formation of V_k centers (or, Br₂[−] dimers).^[112] Doping of $Cs_2\Box SnCl_6$ nanocrystals with antimony leads to an additional low-energy emission band, ascribed to triplet-state self-trapped excitons,^[173] and a combination of Raman spectroscopy and fitting of PL linewidths found intermediate electron–phonon coupling strengths in $Cs_2\Box SnI_6$.^[174] The inclusion of larger cations at the A-site in $A_2\Box SnI_6$ (A = Cs, MA, FA) leads to increased lattice anharmonicity and octahedral tilting, caused by changes in the interoctahedral I–I distances, leading to more tightly bound polarons and lower polaron mobilities.^[74] Although some of the vacancy-ordered metal halides show quite dispersive band structures, indicative of lower charge-carrier effective

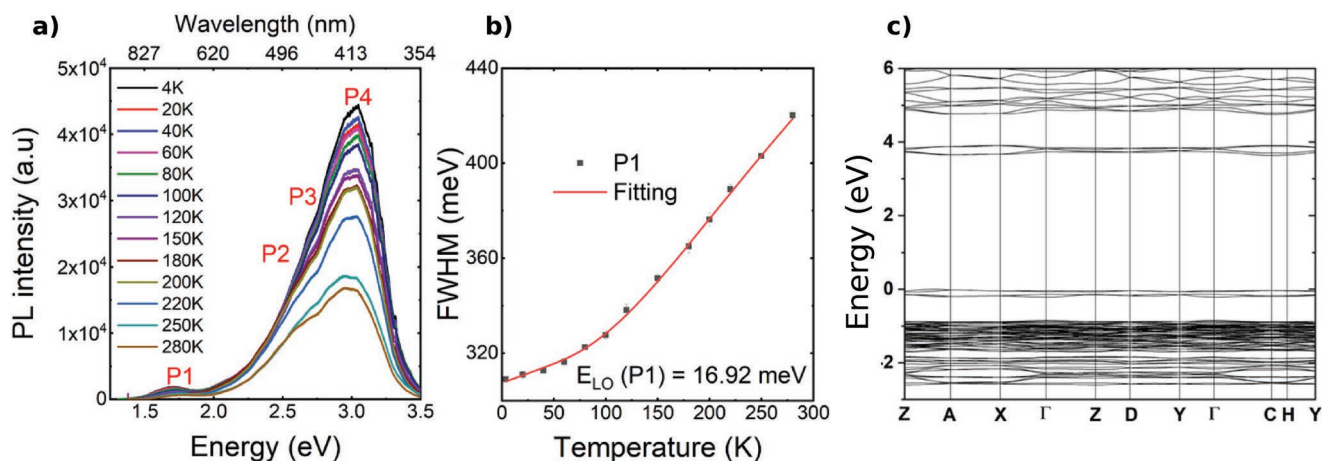


Figure 7. Photoluminescence measurements and DFT calculations for the quasi-0D metal-halide (DETA)PbCl₅·H₂O by Yangui et al.^[180] illustrative of the behavior observed across many quasi 0D metal-halide semiconductors. a) Temperature-dependent spectra between 4–280 K, with four emissive species P1–P4 identified. P1 is attributed to emission from a self-trapped exciton localized on the [Pb₂Cl₁₀]⁶⁻ bi-octahedra. b) Fit of the full-width half-maximum of the P1 peak, following the procedure outlined by Wright et al.^[79] The fit gives an LO phonon energy of 16.9 meV, matching a measured Raman mode at 137 cm⁻¹ (17.0 meV), and also gives a very large electron–phonon coupling constant of $\gamma_{LO} = 385 \text{ meV K}^{-1}$.^{[180][79]} c) Band structure calculated for (DETA)PbCl₅·H₂O using the PBE functional.^[180] The bands are highly non-dispersive, which typically indicates a higher likelihood of charge-carrier localization. Adapted with permission.^[180] Copyright 2019, American Chemical Society.

masses and higher mobilities,^[26,77,171] the high likelihood of lattice distortion in many vacancy-ordered perovskites is conducive to polaron formation and strong charge localization,^[10,77,170] making it difficult for these materials to be used in photovoltaic applications where good charge transport is crucial.

4.5.2. Quasi-0D Metal-Halides

Quasi-0D metal-halides also tend to display strong localization effects, which can be traced back to their structures having easily-distorted individual metal-halide octahedra or similar structural units. Electronically one would expect them to behave analogously to very small nanocrystals, that is, charges are strongly confined and become spatially localized easily.^[71,175,176] Materials with chemical formula A₄BX₆, where A is a large organic cation, have isolated [BX₆] octahedra (shown in Figure 2f).^[168,175] For example, in single-crystal (C₈NH₁₂)₄Bi_{0.57}Sb_{0.43}Br₇·H₂O the structure has both [BiBr₆]³⁻ and [SbBr₆]³⁻ octahedral units separated by the larger organic cations;^[177] in fully inorganic Cs₄(Sn/Pb)Br₆ the [(Sn/Pb)Br₆]⁴⁻ octahedra are separated by Cs⁺ cations;^[12,31,178,179] and in (DETA)PbCl₅·H₂O (DETA = diethylenetriammonium) bi-octahedral units of [Pb₂Cl₁₀]⁶⁻ form (see Figure 7).^[180] Slightly different structures arise in (C₉NH₂₀)₂SbCl₅, which has isolated quadrangular [SbCl₅]²⁻ pyramids (shown in Figure 2g);^[176] Cs₃Cu₂I₅, which has tetragonal and trigonal [Cu₂I₅]³⁻ sites;^[181,182] and (Bmpip)₂MX₄ (Bmpip = 1-butyl-1-methylpiperidinium; M = Ge, Sn, Pb; X = Br, I), which forms isolated disphenoidal [MX₄]²⁻ anions.^[183] Beyond this, a variety of other quasi-0D materials with a range of compositions and structures have been studied, for which self-trapping or charge localization has been attributed as the source of photoluminescence.^[184–188]

A mixture of DFT and photoluminescence-based studies in quasi-0D materials have been used to argue for emission from

polaronic or self-trapped states being prominent, exhibiting typical behavior including large Stokes shifts,^[178,179,183] and longer-lived, narrower PL at low temperatures (see Figure 7a,c for a typical example).^[12,180,181,184] However, as highlighted above, a clear distinction of excitonic and polaronic experimental signals, for example, in ultrafast TA measurements, can be convoluted in 0D systems.^[189] The calculated VBM/CBM electronic bands in quasi-0D metal-halides tend to be highly non-dispersive,^[31,185,187] making charge localization more likely.^[61,62,76] Overall, the broadband, high-efficiency, long-lived PL that is present across many of these materials makes them very promising for applications in lighting or as X-ray scintillators.^[12,168,182] On the other hand, one would expect their isolated structures to inhibit the efficient charge transport and extraction that is crucial for solar cells.^[4]

4.5.3. Other Metal-Halide Semiconductors

Finally, studies of other metal-halide materials also include Rb₄Ag₂BiBr₉, which has a quasi-3D structure involving [BiBr₆] octahedra and [AgBr₅] square pyramids,^[81] and 1D chains of corner-sharing metal-halide octahedra.^[190,191] Sharma et al. used temperature-dependent PL measurements to argue for the presence of multiple self-trapped states contributing to broadband emission in Rb₄Ag₂BiBr₉ (see Figure 3b),^[81] whereas studies of (C₄N₂H₁₄)PbBr₄ and CsCu₂X₃ (X = Cl, Br, I) have identified multiple distinct self-trapped exciton states along 1D chains,^[190,191] leading to broadband light emission in the case of (C₄N₂H₁₄)PbBr₄.^[190]

4.5.4. The Role of Structural Distortion and Low Dimensionality in Non-Perovskite Metal-Halides

The unifying theme for all of the novel non-perovskite metal-halide materials that we discuss here appears to be that,

notwithstanding a wide variety of chemical compositions and crystal structures, these materials often have easily deformable lattices and low-dimensional electronic structures,^[71,76,145] greatly enhancing the likelihood of both structural distortions and charge-carrier localization.^[61,62] This scenario is particularly relevant to quasi-0D metal-halides, as they lack the cohesive crystal structure that stabilizes against distortions.^[12,168] However, so far most studies have relied solely on computational and PL-based measurements for proof of charge-carrier localization; although these materials are more likely to exhibit strong charge-carrier localization effects, further experimental evidence from IR/Raman spectroscopy, ultrafast spectroscopy and charge-carrier mobility measurements would be of great value in identifying the precise origins of these processes.

5. Conclusions and Outlook

We have provided an overview of current understanding of polarons and localization effects across a wide variety of metal-halide semiconductors. In the case of ubiquitous 3D metal-halide perovskites, there is widespread consensus around the dominant role of Fröhlich couplings leading to the formation of large polarons.^[50,79] Polaron formation is fast, occurring within hundreds of fs, and the organic cation plays little to no role in this process.^[104,109] Compositional tuning of the halide alters polaronic effects, with bromide giving much stronger couplings than iodide.^[79,130] Replacement of lead with tin might lead to changes in charge–lattice couplings, although the full impact is not yet clear, given that some of the fundamental changes in optoelectronic properties may still be obscured by extrinsic effects deriving from high defect densities and poor crystallinity in tin-based MHPs.^[96,132,133] The role of lattice anharmonicity in MHPs is still the subject of some debate,^[24,32,60] and detailed experimental studies, for example using magneto-absorption spectroscopy or electron paramagnetic resonance, which can provide valuable insights into polaron energy levels, transport and interactions with the local lattice structure,^[49,115,192,193] could help to clarify which modeling approach is more suitable for understanding the fundamental properties of MHPs. Overall, polarons in metal-halide perovskites have little detrimental impact, and thus high-performance solar cell devices have indeed been developed based on these materials.

Ruddlesden–Popper layered perovskites are the “edge case” of small polaron behavior, with several experimental studies of these materials indicating the presence of strong charge–lattice interactions,^[8,106] although there are several other competing processes that might play a role in these materials including defect-mediated recombination, exciton formation and structural distortions.^[35,164] Understanding clearly why certain types of Ruddlesden–Popper perovskites have sharp, efficient emission at low Stokes shift whereas others exhibit broadband PL at large Stokes shifts, and which compositional or structural parameters can be tuned to alter this, will be valuable in developing their application, especially for LEDs. Studies of non-perovskite metal-halide materials, from vacancy-ordered semiconductors through to 0D metal-halides, have to date mainly made use of DFT calculations and photoluminescence-based experiments to indicate the presence of strong

charge-carrier localization.^[10,12,71] These materials tend to show highly non-dispersive electronic bands^[26,187] and highly efficient, broad emission at large Stokes shifts,^[12,168] which point toward polaron formation and charge-carrier self-trapping.

Overall, we find that there is still plenty of scope for experimental studies of new metal-halide semiconductors, ideally using IR, Raman or OPTP spectroscopies to better understand the precise nature of charge-carrier localization and its influence on optoelectronic properties. Given the wide range of possible materials, focusing research onto a few “prototypical” metal-halide systems could be of great help in clarifying common properties of some of these materials, as has been done with MAPbI₃ with respect to MHPs. Thus, research should focus on model vacancy-ordered materials with formula A₃□B₂³⁺X₉ and A₂□B⁴⁺X₆, and the 0D metal-halide A₄BX₆. Ideally, such work would center around materials that included the same metal and halide elements, allowing for easier comparisons to be made. Alternatively, given the ease of compositional variation across double perovskites, these could be good model systems for studying the correlation between electronic dimensionality, structural dimensionality, and charge-carrier localization. Such studies would help to clarify fundamental questions around whether charge-carrier localization is linked to the peculiar lattice structure of many metal-halide materials,^[10,26,71] or whether the role of low-dimensional electronic structures is more critical.^[76,145] Further work might also clarify whether structural distortion in a material can be used as an impactful way to tune its optoelectronic properties, which would provide a new window into materials design and selection.^[74,120] Such research would set a clear pathway toward identification of the most promising material systems for future investigation and application in optoelectronic devices.

There is clear demand for new semiconducting materials applied to energy innovation, from efficient white-light emitting LEDs^[8,37] to lead-free, non-toxic solar cells^[7,26] that make use of earth-abundant materials with low environmental footprints.^[194,195] Thus, establishing a rigorous and methodical approach to exploring this wide range of new metal-halide semiconductors will be crucial to ensuring that research can focus on those materials best suited to specific applications. As we have outlined here, identifying and characterising polaronic behavior is complex, requiring multiple complementary experimental signatures, yet it is also fundamental to understanding charge-carrier transport and dynamics in a material, and thus judging its effectiveness for a particular optoelectronic device. There are several potential pitfalls in such work. First, multiple processes can lead to similar experimental signals, as in transient absorption decays. Second, carrying out only one kind of steady-state measurement, such as PL or optical absorption, is often not enough to provide definitive evidence for charge-carrier localization. Third, disentangling which processes lead to polaron formation can prove fiendishly difficult. Nonetheless, it is clear that there are many varied, fascinating and potentially useful materials that are only at the start of being investigated and understood. Innovative material selection and characterization, along with careful, strategic approaches across this field of research will be necessary to drive continued exploration of new metal-halide semiconductors for energy applications.

Acknowledgements

The authors are thankful to the Engineering and Physical Sciences Research Council (EPSRC) for financial support. L.R.V.B acknowledges funding from the EPSRC Centre for Doctoral Training in New and Sustainable Photovoltaics and the Oxford-Radcliffe Scholarship. L.M.H thanks TUM-IAS for a Hans Fischer Senior Fellowship.

Conflict of Interest

The authors declare no conflict of interest.

Keywords

charge-carrier localization, metal halides, optoelectronic devices, perovskites, polarons, semiconducting materials

Received: October 16, 2020

Revised: December 2, 2020

Published online:

- [1] M. A. Green, A. Ho-Baillie, H. J. Snaith, *Nat. Photonics* **2014**, *8*, 506.
- [2] L. Protesescu, S. Yakunin, M. I. Bodnarchuk, F. Krieg, R. Caputo, C. H. Hendon, R. X. Yang, A. Walsh, M. V. Kovalenko, *Nano Lett.* **2015**, *15*, 3692.
- [3] L. M. Herz, *ACS Energy Lett.* **2017**, *2*, 1539.
- [4] M. B. Johnston, L. M. Herz, *Acc. Chem. Res.* **2016**, *49*, 146.
- [5] Best Research-Cell Efficiency Chart | Photovoltaic Research | NREL, <https://www.nrel.gov/pv/cell-efficiency.html> (accessed: October 2020).
- [6] S. Li, J. Luo, J. Liu, J. Tang, *J. Phys. Chem. Lett.* **2019**, *10*, 1999.
- [7] M. R. Filip, F. Giustino, *Proc. Natl. Acad. Sci. USA* **2018**, *115*, 5397.
- [8] M. D. Smith, H. I. Karunadasa, *Acc. Chem. Res.* **2018**, *51*, 619.
- [9] H. Tsai, W. Nie, J.-C. Blancon, C. C. Stoumpos, R. Asadpour, B. Harutyunyan, A. J. Neukirch, R. Verduzco, J. J. Crochet, S. Tretiak, L. Pedesseau, J. Even, M. A. Alam, G. Gupta, J. Lou, P. M. Ajayan, M. J. Bedzyk, M. G. Kanatzidis, A. D. Mohite, *Nature* **2016**, *536*, 312.
- [10] K. M. McCall, C. C. Stoumpos, S. S. Kostina, M. G. Kanatzidis, B. W. Wessels, *Chem. Mater.* **2017**, *29*, 4129.
- [11] S. J. Zelewski, J. M. Urban, A. Surrente, D. K. Maude, A. Kuc, L. Schade, R. D. Johnson, M. Dollmann, P. K. Nayak, H. J. Snaith, P. Radaelli, R. Kudrawiec, R. J. Nicholas, P. Plochocka, M. Baranowski, *J. Mater. Chem. C* **2019**, *7*, 8350.
- [12] B. M. Benin, D. N. Dirin, V. Morad, M. Wörle, S. Yakunin, G. Rainò, O. Nazarenko, M. Fischer, I. Infante, M. V. Kovalenko, *Angew. Chem., Int. Ed.* **2018**, *57*, 11329.
- [13] Y. He, G. Galli, *Chem. Mater.* **2014**, *26*, 5394.
- [14] T. Saito, T. Iwasaki, S. Kurosawa, A. Yoshikawa, T. Den, *Nucl. Instrum. Methods Phys. Res., Sect. A* **2016**, *806*, 395.
- [15] L. D. Landau, *Phys. Z. Sowjetunion* **1933**, *3*, 644.
- [16] S. Pekar, *Zh. Eksp. Teor. Fiz.* **1946**, *16*, 347.
- [17] T. Holstein, *Ann. Phys.* **1959**, *8*, 343.
- [18] R. P. Feynman, *Phys. Rev.* **1955**, *97*, 660.
- [19] W. Rehman, D. P. McMeekin, J. B. Patel, R. L. Milot, M. B. Johnston, H. J. Snaith, L. M. Herz, *Chemistry Environ. Sci.* **2017**, *10*, 361.
- [20] Z. Wang, Q. Lin, F. P. Chmiel, N. Sakai, L. M. Herz, H. J. Snaith, *Nat. Energy* **2017**, *2*, 17135.
- [21] J. M. Frost, *Phys. Rev. B* **2017**, *96*, 195202.
- [22] M. Sendner, P. K. Nayak, D. A. Egger, S. Beck, C. Müller, B. Epding, W. Kowalsky, L. Kronik, H. J. Snaith, A. Pucci, R. Lovrinčić, *Mater. Horiz.* **2016**, *3*, 613.
- [23] K. T. Munson, J. R. Swartzfager, J. B. Asbury, *ACS Energy Lett.* **2019**, *4*, 1888.
- [24] D. A. Egger, A. Bera, D. Cahen, G. Hodes, T. Kirchartz, L. Kronik, R. Lovrinčić, A. M. Rappe, D. R. Reichman, O. Yaffe, *Adv. Mater.* **2018**, *30*, 1800691.
- [25] D. Meggiolaro, F. Ambrosio, E. Mosconi, A. Mahata, F. De Angelis, *Adv. Energy Mater.* **2020**, *10*, 1902748.
- [26] F. Giustino, H. J. Snaith, *ACS Energy Lett.* **2016**, *1*, 1233.
- [27] D. P. McMeekin, G. Sadoughi, W. Rehman, G. E. Eperon, M. Saliba, M. T. Horantner, A. Haghighirad, N. Sakai, L. Korte, B. Rech, M. B. Johnston, L. M. Herz, H. J. Snaith, *Science* **2016**, *351*, 151.
- [28] A. H. Slavney, T. Hu, A. M. Lindenberg, H. I. Karunadasa, *J. Am. Chem. Soc.* **2016**, *138*, 7.
- [29] E. T. McClure, M. R. Ball, W. Windl, P. M. Woodward, *Chem. Mater.* **2016**, *28*, 1348.
- [30] T. M. Koh, V. Shanmugam, J. Schlipf, L. Oesinghaus, P. Müller-Buschbaum, N. Ramakrishnan, V. Swamy, N. Mathews, P. P. Boix, S. G. Mhaisalkar, *Adv. Mater.* **2016**, *28*, 3653.
- [31] B. Kang, K. Biswas, *J. Phys. Chem. Lett.* **2018**, *9*, 830.
- [32] M. Schlipf, S. Poncé, F. Giustino, *Phys. Rev. Lett.* **2018**, *121*, 086402.
- [33] S. Poncé, M. Schlipf, F. Giustino, *ACS Energy Lett.* **2019**, *4*, 456.
- [34] R. Williams, K. Song, *J. Phys. Chem. Solids* **1990**, *51*, 679.
- [35] D. Cortecchia, J. Yin, A. Petrozza, C. Soci, *J. Mater. Chem. C* **2019**, *7*, 4956.
- [36] C. Dotzler, G. V. M. Williams, A. Edgar, S. Schweizer, B. Henke, J. M. Spaeth, A. Bittar, J. Hamlin, C. Dunford, *J. Appl. Phys.* **2006**, *100*, 033102.
- [37] Y. Kim, J. S. Kim, T. Lee, *Adv. Mater.* **2019**, *31*, 1804595.
- [38] Q. V. Le, H. W. Jang, S. Y. Kim, *Small Methods* **2018**, *2*, 1700419.
- [39] X. K. Liu, W. Xu, S. Bai, Y. Jin, J. Wang, R. H. Friend, F. Gao, *Nat. Mater.* **2021**, *20*, 10.
- [40] H. Wei, J. Huang, *Nat. Commun.* **2019**, *10*, 1066.
- [41] G. Kakavelakis, M. Gedda, A. Panagiotopoulos, E. Kymakis, T. D. Anthopoulos, K. Petridis, *Adv. Sci.* **2020**, *7*, 2002098.
- [42] L. D. Landau, S. I. Pekar, *Zh. Eksp. Teor. Fiz* **1948**, *18*, 419.
- [43] H. Fröhlich, H. Pelzer, S. Zienau, *London Edinburgh Philos. Mag. J. Sci.* **1950**, *41*, 221.
- [44] H. Fröhlich, *Adv. Phys.* **1954**, *3*, 325.
- [45] R. P. Feynman, R. W. Hellwarth, C. K. Iddings, P. M. Platzman, *Phys. Rev.* **1962**, *127*, 1004.
- [46] Y. Ōsaka, *Prog. Theor. Phys.* **1959**, *22*, 437.
- [47] Y. Ōsaka, *Prog. Theor. Phys.* **1961**, *25*, 517.
- [48] J. T. Marshall, L. R. Mills, *Phys. Rev. B* **1970**, *2*, 3143.
- [49] J. T. Devreese, A. S. Alexandrov, *Rep. Prog. Phys.* **2009**, *72*, 066501.
- [50] L. M. Herz, *J. Phys. Chem. Lett.* **2018**, *9*, 6853.
- [51] R. W. Hellwarth, I. Biaggio, *Phys. Rev. B* **1999**, *60*, 299.
- [52] O. Yaffe, Y. Guo, L. Z. Tan, D. A. Egger, T. Hull, C. C. Stoumpos, F. Zheng, T. F. Heinz, L. Kronik, M. G. Kanatzidis, J. S. Owen, A. M. Rappe, M. A. Pimenta, L. E. Brus, *Phys. Rev. Lett.* **2017**, *118*, 136001.
- [53] M. Z. Mayers, L. Z. Tan, D. A. Egger, A. M. Rappe, D. R. Reichman, *Nano Lett.* **2018**, *18*, 8041.
- [54] Y. Toyozawa, *Prog. Theor. Phys.* **1961**, *26*, 29.
- [55] Y. Toyozawa, *J. Phys. Soc. Jpn.* **1978**, *44*, 482.
- [56] K. S. Song, R. T. Williams, *Self-Trapped Excitons*, Springer, Berlin, Germany **1993**.
- [57] P. Tasker, A. Stoneham, *J. Phys. Chem. Solids* **1977**, *38*, 1185.
- [58] A. M. Stoneham, J. Gavartin, A. L. Shluger, A. V. Kimmel, D. Műoz Ramo, H. M. Rønnow, G. Aeppli, C. Renner, *J. Phys.: Condens. Matter* **2007**, *19*, 255208.
- [59] F. Bridges, G. Davies, J. Robertson, A. M. Stoneham, *J. Phys.: Condens. Matter* **1990**, *2*, 2875.
- [60] W. H. Sio, C. Verdi, S. Poncé, F. Giustino, *Phys. Rev. B* **2019**, *99*, 235139.
- [61] D. Emin, T. Holstein, *Phys. Rev. Lett.* **1976**, *36*, 323.

- [62] V. V. Kabanov, O. Y. Mashtakov, *Phys. Rev. B* **1993**, *47*, 6060.
- [63] N. F. Mott, A. M. Stoneham, *J. Phys. C: Solid State Phys.* **1977**, *10*, 3391.
- [64] Y. Unuma, Y. Masumoto, S. Shionoya, H. Nishimura, *J. Phys. Soc. Jpn.* **1983**, *52*, 4277.
- [65] F. X. Morrissey, J. G. Mance, A. D. Van Pelt, S. L. Dexheimer, *J. Phys.: Condens. Matter* **2013**, *25*, 144204.
- [66] S. Tomimoto, H. Nansei, S. Saito, T. Suemoto, J. Takeda, S. Kurita, *Phys. Rev. Lett.* **1998**, *81*, 417.
- [67] F. Giustino, *Rev. Mod. Phys.* **2017**, *89*, 015003.
- [68] W. H. Sio, C. Verdi, S. Poncé, F. Giustino, *Phys. Rev. Lett.* **2019**, *122*, 246403.
- [69] D. Zhao, J. M. Skelton, H. Hu, C. La-o vorakiat, J.-X. Zhu, R. A. Marcus, M.-E. Michel-Beyerle, Y. M. Lam, A. Walsh, E. E. M. Chia, *Appl. Phys. Lett.* **2017**, *111*, 201903.
- [70] Y. Lan, B. J. Dringoli, D. A. Valverde-Chávez, C. S. Ponseca, M. Sutton, Y. He, M. G. Kanatzidis, D. G. Cooke, *Sci. Adv.* **2019**, *5*, eaaw5558.
- [71] H. Lin, C. Zhou, Y. Tian, T. Siegrist, B. Ma, *ACS Energy Lett.* **2017**, *3*, 54.
- [72] J. Yin, H. Li, D. Cortecchia, C. Soci, J.-L. Brédas, *ACS Energy Lett.* **2017**, *2*, 417.
- [73] A. R. Srimath Kandada, C. Silva, *J. Phys. Chem. Lett.* **2020**, *11*, 3173.
- [74] A. E. Maughan, A. M. Ganose, A. M. Candia, J. T. Granger, D. O. Scanlon, J. R. Neilson, *Chem. Mater.* **2018**, *30*, 472.
- [75] A. E. Maughan, A. M. Ganose, M. A. Almaker, D. O. Scanlon, J. R. Neilson, *Chem. Mater.* **2018**, *30*, 3909.
- [76] Z. Xiao, W. Meng, J. Wang, D. B. Mitzi, Y. Yan, *Mater. Horiz.* **2017**, *4*, 206.
- [77] Z. Xiao, Z. Song, Y. Yan, *Adv. Mater.* **2019**, *31*, 1803792.
- [78] P. Y. Yu, M. Cardona, *Fundamentals of Semiconductors: Physics and Materials Properties*, 4th ed., Springer, New York **2010**.
- [79] A. D. Wright, C. Verdi, R. L. Milot, G. E. Eperon, M. A. Pérez-Osorio, H. J. Snaith, F. Giustino, M. B. Johnston, L. M. Herz, *Nat. Commun.* **2016**, *7*, 11755.
- [80] D. Emin, *Phys. Rev. B* **1993**, *48*, 13691.
- [81] M. Sharma, A. Yangui, V. R. Whiteside, I. R. Sellers, D. Han, S. Chen, M.-H. Du, B. Sagarov, *Inorg. Chem.* **2019**, *58*, 4446.
- [82] K. Huang, A. Rhys, *Proc. R. Soc. London, Ser. A* **1950**, *204*, 406.
- [83] M. De Jong, L. Seijo, A. Meijerink, F. T. Rabouw, *Phys. Chem. Chem. Phys.* **2015**, *17*, 16959.
- [84] S. Neutzner, F. Thouin, D. Cortecchia, A. Petrozza, C. Silva, A. R. S. Kandada, *Phys. Rev. Mater.* **2018**, *2*, 064605.
- [85] S. Kahmann, E. K. Tekelenburg, H. Duim, M. E. Kamminga, M. A. Loi, *Nat. Commun.* **2020**, *11*, 2344.
- [86] I. Studenyak, M. Kranjec, M. Kurik, *Int. J. Opt. Appl.* **2014**, *4*, 76.
- [87] N. K. Noel, B. Wenger, S. N. Habisreutinger, J. B. Patel, T. Crothers, Z. Wang, R. J. Nicholas, M. B. Johnston, L. M. Herz, H. J. Snaith, *ACS Energy Lett.* **2018**, *3*, 1233.
- [88] J. M. Richter, M. Abdi-Jalebi, A. Sadhanala, M. Tabachnyk, J. P. Rivett, L. M. Pazos-Outón, K. C. Gödel, M. Price, F. Deschler, R. H. Friend, *Nat. Commun.* **2016**, *7*, 13941.
- [89] S. Rudin, T. L. Reinecke, B. Segall, *Phys. Rev. B* **1990**, *42*, 11218.
- [90] S. Kahmann, S. Shao, M. A. Loi, *Adv. Funct. Mater.* **2019**, *29*, 1902963.
- [91] E. R. Dohner, A. Jaffe, L. R. Bradshaw, H. I. Karunadasa, *J. Am. Chem. Soc.* **2014**, *136*, 13154.
- [92] J. U. Fischbach, D. Fröhlich, M. N. Kabler, *J. Lumin.* **1973**, *6*, 29.
- [93] D. Emin, *Phys. Rev. B* **1971**, *4*, 3639.
- [94] R. L. Milot, G. E. Eperon, H. J. Snaith, M. B. Johnston, L. M. Herz, *Adv. Funct. Mater.* **2015**, *25*, 6218.
- [95] H. T. Yi, X. Wu, X. Zhu, V. Podzorov, *Adv. Mater.* **2016**, *28*, 6509.
- [96] R. L. Milot, M. T. Klug, C. L. Davies, Z. Wang, H. Kraus, H. J. Snaith, M. B. Johnston, L. M. Herz, *Adv. Mater.* **2018**, *30*, 1804506.
- [97] E. M. Hutter, M. C. Gélvez-Rueda, D. Bartesaghi, F. C. Grozema, T. J. Savenije, *ACS Omega* **2018**, *3*, 11655.
- [98] C. L. Davies, J. Borchert, C. Q. Xia, R. L. Milot, H. Kraus, M. B. Johnston, L. M. Herz, *J. Phys. Chem. Lett.* **2018**, *9*, 4502.
- [99] M. A. Pérez-Osorio, R. L. Milot, M. R. Filip, J. B. Patel, L. M. Herz, M. B. Johnston, F. Giustino, *J. Phys. Chem. C* **2015**, *119*, 25703.
- [100] K. T. Munson, E. R. Kennehan, G. S. Doucette, J. B. Asbury, *Chem* **2018**, *4*, 2826.
- [101] F. Thouin, D. A. Valverde-Chávez, C. Quarti, D. Cortecchia, I. Bargigia, D. Beljonne, A. Petrozza, C. Silva, A. R. S. Kandada, *Nat. Mater.* **2019**, *18*, 349.
- [102] C. Wehrenfennig, G. E. Eperon, M. B. Johnston, H. J. Snaith, L. M. Herz, *Adv. Mater.* **2014**, *26*, 1584.
- [103] E. Cinquanta, D. Meggiolaro, S. G. Motti, M. Gandini, M. J. P. Alcocer, Q. A. Akkerman, C. Vozi, L. Manna, F. De Angelis, A. Petrozza, S. Stagira, *Phys. Rev. Lett.* **2019**, *122*, 166601.
- [104] S. A. Bretschneider, I. Ivanov, H. I. Wang, K. Miyata, X. Zhu, M. Bonn, *Adv. Mater.* **2018**, *30*, 1707312.
- [105] D. Zhao, E. E. M. Chia, *Adv. Opt. Mater.* **2020**, *8*, 1900783.
- [106] D. Cortecchia, J. Yin, A. Bruno, S.-Z. A. Lo, G. G. Gurzadyan, S. Mhaisalkar, J.-L. Brédas, C. Soci, *J. Mater. Chem. C* **2017**, *5*, 2771.
- [107] J. Fu, Q. Xu, G. Han, B. Wu, C. H. A. Huan, M. L. Leek, T. C. Sum, *Nat. Commun.* **2017**, *8*, 1300.
- [108] G. Batignani, G. Fumero, A. R. Srimath Kandada, G. Cerullo, M. Gandini, C. Ferrante, A. Petrozza, T. Scopigno, *Nat. Commun.* **2018**, *9*, 1971.
- [109] K. T. Munson, J. R. Swartzfager, J. Gan, J. B. Asbury, *J. Phys. Chem. Lett.* **2020**, *11*, 3166.
- [110] H. Zhu, K. Miyata, Y. Fu, J. Wang, P. P. Joshi, D. Niesner, K. W. Williams, S. Jin, X.-Y. Zhu, *Science* **2016**, *353*, 1409.
- [111] D. M. Monahan, L. Guo, J. Lin, L. Dou, P. Yang, G. R. Fleming, *J. Phys. Chem. Lett.* **2017**, *8*, 3211.
- [112] C. Liu, Y. Wang, H. Geng, T. Zhu, E. Ertekin, D. Gosztola, S. Yang, J. Huang, B. Yang, K. Han, S. E. Canton, Q. Kong, K. Zheng, X. Zhang, *J. Am. Chem. Soc.* **2019**, *141*, 13074.
- [113] K. Zheng, M. Abdellah, Q. Zhu, Q. Kong, G. Jennings, C. A. Kurtz, M. E. Messing, Y. Niu, D. J. Gosztola, M. J. Al-Marri, X. Zhang, T. Pullerits, S. E. Canton, *J. Phys. Chem. Lett.* **2016**, *7*, 4535.
- [114] C. Liu, H. Tsai, W. Nie, D. J. Gosztola, X. Zhang, *J. Phys. Chem. Lett.* **2020**, *11*, 6256.
- [115] F. M. Peeters, J. T. Devreese, *Phys. Rev. B* **1986**, *34*, 7246.
- [116] J. W. Hodby, G. P. Russell, F. M. Peeters, J. T. Devreese, D. M. Larsen, *Phys. Rev. Lett.* **1987**, *58*, 1471.
- [117] A. Miyata, A. Mitioglu, P. Plochocka, O. Portugall, J. T. W. Wang, S. D. Stranks, H. J. Snaith, R. J. Nicholas, *Nat. Phys.* **2015**, *11*, 582.
- [118] K. Galkowski, A. Surrente, M. Baranowski, B. Zhao, Z. Yang, A. Sadhanala, S. Mackowski, S. D. Stranks, P. Plochocka, *ACS Energy Lett.* **2019**, *4*, 615.
- [119] J. C. Blancon, A. V. Stier, H. Tsai, W. Nie, C. C. Stoumpos, B. Traoré, L. Pedesseau, M. Kepenekian, F. Katsutani, G. T. Noe, J. Kono, S. Tretiak, S. A. Crooker, C. Katan, M. G. Kanatzidis, J. J. Crochet, J. Even, A. D. Mohite, *Nat. Commun.* **2018**, *9*, 2254.
- [120] J. M. Urban, G. Chehade, M. Dyksik, M. Menahem, A. Surrente, G. Trippé-Allard, D. K. Maude, D. Garrot, O. Yaffe, E. Deleporte, P. Plochocka, M. Baranowski, *J. Phys. Chem. Lett.* **2020**, *11*, 5830.
- [121] M. Baranowski, P. Plochocka, *Adv. Energy Mater.* **2020**, *10*, 1903659.
- [122] M. Dyksik, H. Duim, X. Zhu, Z. Yang, M. Gen, Y. Kohama, S. Adjokatse, D. K. Maude, M. A. Loi, D. A. Egger, M. Baranowski, P. Plochocka, *ACS Energy Lett.* **2020**, *5*, 3609.
- [123] T. Zhao, W. Shi, J. Xi, D. Wang, Z. Shuai, *Sci. Rep.* **2016**, *6*, 19968.
- [124] A. Kojima, K. Teshima, Y. Shirai, T. Miyasaka, *J. Am. Chem. Soc.* **2009**, *131*, 6050.
- [125] T. Baikie, Y. Fang, J. M. Kadro, M. Schreyer, F. Wei, S. G. Mhaisalkar, M. Graetzel, T. J. White, *J. Mater. Chem. A* **2013**, *1*, 5628.

- [126] L. D. Whalley, J. M. Skelton, J. M. Frost, A. Walsh, *Phys. Rev. B* **2016**, *94*, 220301.
- [127] C. Gehrman, D. A. Egger, *Nat. Commun.* **2019**, *10*, 3141.
- [128] A. Mahata, D. Meggiolaro, F. De Angelis, *J. Phys. Chem. Lett.* **2019**, *10*, 1790.
- [129] A. J. Neukirch, W. Nie, J.-C. Blancon, K. Appavoo, H. Tsai, M. Y. Sfeir, C. Katan, L. Pedesseau, J. Even, J. J. Crochet, G. Gupta, A. D. Mohite, S. Tretiak, *Nano Lett.* **2016**, *16*, 3809.
- [130] A. J. Neukirch, I. I. Abate, L. Zhou, W. Nie, H. Tsai, L. Pedesseau, J. Even, J. J. Crochet, A. D. Mohite, C. Katan, S. Tretiak, *J. Phys. Chem. Lett.* **2018**, *9*, 7130.
- [131] A. Filippetti, A. Mattoni, C. Caddeo, M. I. Saba, P. Delugas, *Phys. Chem. Chem. Phys.* **2016**, *18*, 15352.
- [132] K. J. Savill, A. M. Ulatowski, M. D. Farrar, M. B. Johnston, H. J. Snaith, L. M. Herz, *Adv. Funct. Mater.* **2020**, *30*, 2005594.
- [133] M. T. Klug, R. L. Milot, J. Patel, T. Green, H. C. Sansom, M. Farrar, A. J. Ramadan, S. Martani, Z. Wang, B. Wenger, J. M. Ball, L. Langshaw, A. Petrozza, M. B. Johnston, L. M. Herz, H. Snaith, *Energy Environ. Sci.* **2020**, *13*, 1776.
- [134] N. K. Noel, S. D. Stranks, A. Abate, C. Wehrenfennig, S. Guarnera, A.-A. Haghighirad, A. Sadhanala, G. E. Eperon, S. K. Pathak, M. B. Johnston, A. Petrozza, L. M. Herz, H. J. Snaith, *Energy Environ. Sci.* **2014**, *7*, 3061.
- [135] S. G. Motti, F. Krieg, A. J. Ramadan, J. B. Patel, H. J. Snaith, M. V. Kovalenko, M. B. Johnston, L. M. Herz, *Adv. Funct. Mater.* **2020**, *30*, 1909904.
- [136] Q. Zhao, A. Hazarika, L. T. Schelhas, J. Liu, E. A. Gaulding, G. Li, M. Zhang, M. F. Toney, P. C. Sercel, J. M. Luther, *ACS Energy Lett.* **2020**, *5*, 238.
- [137] S. C. Boehme, S. ten Brinck, J. Maes, N. Yazdani, F. Zapata, K. Chen, V. Wood, J. M. Hodgkiss, Z. Hens, P. Geiregat, I. Infante, *Nano Lett.* **2020**, *20*, 1819.
- [138] F. Ambrosio, D. Meggiolaro, E. Mosconi, F. De Angelis, *ACS Energy Lett.* **2019**, *4*, 2013.
- [139] C. M. Iaru, J. J. Geuchies, P. M. Koenraad, D. Vanmaekelbergh, A. Y. Silov, *ACS Nano* **2017**, *11*, 11024.
- [140] L. Yang, K. Wei, Z. Xu, F. Li, R. Chen, X. Zheng, X. Cheng, T. Jiang, *Opt. Lett.* **2018**, *43*, 122.
- [141] J. Li, X. Yuan, P. Jing, J. Li, M. Wei, J. Hua, J. Zhao, L. Tian, *RSC Adv.* **2016**, *6*, 78311.
- [142] A. D. Wright, G. Volonakis, J. Borchert, C. L. Davies, F. Giustino, M. B. Johnston, L. M. Herz, *Nat. Mater.* **2020**, *19*, 1201.
- [143] G. Volonakis, M. R. Filip, A. A. Haghighirad, N. Sakai, B. Wenger, H. J. Snaith, F. Giustino, *J. Phys. Chem. Lett.* **2016**, *7*, 1254.
- [144] M. R. Filip, S. Hillman, A. A. Haghighirad, H. J. Snaith, F. Giustino, *J. Phys. Chem. Lett.* **2016**, *7*, 2579.
- [145] X.-G. Zhao, D. Yang, J.-C. Ren, Y. Sun, Z. Xiao, L. Zhang, *Joule* **2018**, *2*, 1662.
- [146] H. Shi, M. H. Du, *Phys. Rev. Appl.* **2015**, *3*, 054005.
- [147] G. Volonakis, A. A. Haghighirad, R. L. Milot, W. H. Sio, M. R. Filip, B. Wenger, M. B. Johnston, L. M. Herz, H. J. Snaith, F. Giustino, *J. Phys. Chem. Lett.* **2017**, *8*, 772.
- [148] J. A. Steele, P. Puech, M. Keshavarz, R. Yang, S. Banerjee, E. Debroye, C. W. Kim, H. Yuan, N. H. Heo, J. Vanacken, A. Walsh, J. Hofkens, M. B. Roeffaers, *ACS Nano* **2018**, *12*, 8081.
- [149] J. Luo, X. Wang, S. Li, J. Liu, Y. Guo, G. Niu, L. Yao, Y. Fu, L. Gao, Q. Dong, C. Zhao, M. Leng, F. Ma, W. Liang, L. Wang, S. Jin, J. Han, L. Zhang, J. Etheridge, J. Wang, Y. Yan, E. H. Sargent, J. Tang, *Nature* **2018**, *563*, 541.
- [150] R. Zeng, L. Zhang, Y. Xue, B. Ke, Z. Zhao, D. Huang, Q. Wei, W. Zhou, B. Zou, *J. Phys. Chem. Lett.* **2020**, *11*, 2053.
- [151] B. Yang, F. Hong, J. Chen, Y. Tang, L. Yang, Y. Sang, X. Xia, J. Guo, H. He, S. Yang, W. Deng, K. Han, *Angew. Chem., Int. Ed.* **2019**, *58*, 2278.
- [152] D. Manna, J. Kangsabanik, T. K. Das, D. Das, A. Alam, A. Yella, *J. Phys. Chem. Lett.* **2020**, *11*, 2113.
- [153] B. A. Connor, L. Leppert, M. D. Smith, J. B. Neaton, H. I. Karunadasa, *J. Am. Chem. Soc.* **2018**, *140*, 5235.
- [154] I. C. Smith, E. T. Hoke, D. Solis-Ibarra, M. D. McGehee, H. I. Karunadasa, *Angew. Chem., Int. Ed.* **2014**, *53*, 11232.
- [155] T. Hu, M. D. Smith, E. R. Dohner, M.-J. Sher, X. Wu, M. T. Trinh, A. Fisher, J. Corbett, X.-Y. Zhu, H. I. Karunadasa, A. M. Lindenberg, *J. Phys. Chem. Lett.* **2016**, *7*, 2258.
- [156] R. L. Milot, R. J. Sutton, G. E. Eperon, A. A. Haghighirad, J. Martinez Hardigree, L. Miranda, H. J. Snaith, M. B. Johnston, L. M. Herz, *Nano Lett.* **2016**, *16*, 7001.
- [157] A. Yangui, D. Garrot, J. S. Lauret, A. Lusson, G. Bouchez, E. Deleporte, S. Pillet, E. E. Bendeif, M. Castro, S. Triki, Y. Abid, K. Boukheddaden, *J. Phys. Chem. C* **2015**, *119*, 23638.
- [158] E. R. Dohner, E. T. Hoke, H. I. Karunadasa, *J. Am. Chem. Soc.* **2014**, *136*, 1718.
- [159] B. Luo, D. Liang, S. Sun, Y. Xiao, X. Lian, X. Li, M.-D. Li, X.-C. Huang, J. Z. Zhang, *J. Phys. Chem. Lett.* **2020**, *11*, 199.
- [160] F. Thouin, A. R. Srimath Kandada, D. A. Valverde-Chávez, D. Cortecchia, I. Bargigia, A. Petrozza, X. Yang, E. R. Bittner, C. Silva, *Chem. Mater.* **2019**, *31*, 7085.
- [161] M. Seitz, A. J. Magdaleno, N. Alcázar-Cano, M. Meléndez, T. J. Lubbers, S. W. Walraven, S. Pakdel, E. Prada, R. Delgado-Buscalioni, F. Prins, *Nat. Commun.* **2020**, *11*, 2035.
- [162] H. Esmailpour, V. R. Whiteside, S. Sourabh, G. E. Eperon, J. T. Precht, M. C. Beard, H. Lu, B. K. Durant, I. R. Sellers, *J. Phys. Chem. C* **2020**, *124*, 9496.
- [163] D. B. Straus, S. H. Parra, N. Iotov, J. Gebhardt, A. M. Rappe, J. E. Subotnik, J. M. Kikkawa, C. R. Kagan, *J. Am. Chem. Soc.* **2016**, *138*, 13798.
- [164] M. D. Smith, B. A. Connor, H. I. Karunadasa, *Chem. Rev.* **2019**, *119*, 3104.
- [165] J. L. Knutson, J. D. Martin, D. B. Mitzi, *Inorg. Chem.* **2005**, *44*, 4699.
- [166] J. Li, J. Wang, J. Ma, H. Shen, L. Li, X. Duan, D. Li, *Nat. Commun.* **2019**, *10*, 806.
- [167] M. D. Birowosuto, D. Cortecchia, W. Drozdowski, K. Brylew, W. Lachmanski, A. Bruno, C. Soci, *Sci. Rep.* **2016**, *6*, 37254.
- [168] C. Zhou, Y. Tian, Z. Yuan, H. Lin, B. Chen, R. Clark, T. Dilbeck, Y. Zhou, J. Hurley, J. Neu, T. Besara, T. Siegrist, P. Djurovich, B. Ma, *ACS Appl. Mater. Interfaces* **2017**, *9*, 44579.
- [169] J. T. Lewis, J. L. Kolopus, E. Sonder, M. M. Abraham, *Phys. Rev. B* **1973**, *7*, 810.
- [170] A. E. Maughan, A. M. Ganose, D. O. Scanlon, J. R. Neilson, *Chem. Mater.* **2019**, *31*, 1184.
- [171] B. Saparov, F. Hong, J. P. Sun, H. S. Duan, W. Meng, S. Cameron, I. G. Hill, Y. Yan, D. B. Mitzi, *Chem. Mater.* **2015**, *27*, 5622.
- [172] A. Kaltzoglou, M. Antoniadou, A. G. Kontos, C. C. Stoumpos, D. Perganti, E. Siranidi, V. Raptis, K. Trohidou, V. Psycharis, M. G. Kanatzidis, P. Falaras, *J. Phys. Chem. C* **2016**, *120*, 11777.
- [173] Y. Jing, Y. Liu, J. Zhao, Z. Xia, *J. Phys. Chem. Lett.* **2019**, *10*, 7439.
- [174] R. Luo, S. Zhang, S. Zhao, J. Li, F. Kang, K. Yu, G. Wei, *Phys. Rev. Appl.* **2020**, *14*, 014048.
- [175] M. I. Saidaminov, O. F. Mohammed, O. M. Bakr, *ACS Energy Lett.* **2017**, *2*, 889.
- [176] C. Zhou, H. Lin, Y. Tian, Z. Yuan, R. Clark, B. Chen, L. J. Van De Burgt, J. C. Wang, Y. Zhou, K. Hanson, Q. J. Meisner, J. Neu, T. Besara, T. Siegrist, E. Lambers, P. Djurovich, B. Ma, *Chem. Sci.* **2018**, *9*, 586.
- [177] R. Zhang, X. Mao, Y. Yang, S. Yang, W. Zhao, T. Wumaier, D. Wei, W. Deng, K. Han, *Angew. Chem., Int. Ed.* **2019**, *58*, 2725.
- [178] J. Yin, P. Maity, M. De Bastiani, I. Dursun, O. M. Bakr, J. L. Brédas, O. F. Mohammed, *Sci. Adv.* **2017**, *3*, e1701793.
- [179] S. Kondo, K. Amaya, T. Saito, *J. Phys.: Condens. Matter* **2002**, *14*, 2093.

- [180] A. Yangui, R. Roccanova, Y. Wu, M.-H. Du, B. Saparov, *J. Phys. Chem. C* **2019**, *123*, 22470.
- [181] T. Jun, K. Sim, S. Iimura, M. Sasase, H. Kamioka, J. Kim, H. Hosono, *Adv. Mater.* **2018**, *30*, 1804547.
- [182] L. Lian, M. Zheng, W. Zhang, L. Yin, X. Du, P. Zhang, X. Zhang, J. Gao, D. Zhang, L. Gao, G. Niu, H. Song, R. Chen, X. Lan, J. Tang, J. Zhang, *Adv. Sci.* **2020**, *7*, 2000195.
- [183] V. Morad, Y. Shynkarenko, S. Yakunin, A. Brumberg, R. D. Schaller, M. V. Kovalenko, *J. Am. Chem. Soc.* **2019**, *141*, 9764.
- [184] C. Zhou, H. Lin, J. Neu, Y. Zhou, M. Chaaban, S. Lee, M. Worku, B. Chen, R. Clark, W. Cheng, J. Guan, P. Djurovich, D. Zhang, X. Lü, J. Bullock, C. Pak, M. Shatruk, M. H. Du, T. Siegrist, B. Ma, *ACS Energy Lett.* **2019**, *4*, 1579.
- [185] C. Zhou, H. Lin, H. Shi, Y. Tian, C. Pak, M. Shatruk, Y. Zhou, P. Djurovich, M.-H. Du, B. Ma, *Angew. Chem.* **2018**, *130*, 1033.
- [186] C. Zhou, H. Lin, M. Worku, J. Neu, Y. Zhou, Y. Tian, S. Lee, P. Djurovich, T. Siegrist, B. Ma, *J. Am. Chem. Soc.* **2018**, *140*, 13181.
- [187] H. Peng, S. Yao, Y. Guo, R. Zhi, X. Wang, F. Ge, Y. Tian, J. Wang, B. Zou, *J. Phys. Chem. Lett.* **2020**, *11*, 4703.
- [188] M. Worku, L. J. Xu, M. Chaaban, A. Ben-Akacha, B. Ma, *APL Mater.* **2020**, *8*, 10902.
- [189] Q. A. Akkerman, A. L. Abdelhady, L. Manna, *J. Phys. Chem. Lett.* **2018**, *9*, 2326.
- [190] Z. Yuan, C. Zhou, Y. Tian, Y. Shu, J. Messier, J. C. Wang, L. J. van de Burgt, K. Kountouriotis, Y. Xin, E. Holt, K. Schanze, R. Clark, T. Siegrist, B. Ma, *Nat. Commun.* **2017**, *8*, 14051.
- [191] M. H. Du, *ACS Energy Lett.* **2020**, *5*, 464.
- [192] S. Yang, A. T. Brant, N. C. Giles, L. E. Halliburton, *Phys. Rev. B: Condens. Matter Mater. Phys.* **2013**, *87*, 125201.
- [193] D. L. Huber, *J. Magn. Magn. Mater.* **2012**, *324*, 2113.
- [194] T. Ibn-Mohammed, S. C. Koh, I. M. Reaney, A. Acquaye, G. Schileo, K. B. Mustapha, R. Greenough, *Renewable Sustainable Energy Rev.* **2017**, *80*, 1321.
- [195] E. Leccisi, V. Fthenakis, *Prog. Energy* **2020**, *2*, 032002.
- [196] M. Puppini, S. Polishchuk, N. Colonna, A. Crepaldi, D. N. Dirin, O. Nazarenko, R. De Gennaro, G. Gatti, S. Roth, T. Barillot, L. Poletto, R. P. Xian, L. Rettig, M. Wolf, R. Ernstorfer, M. V. Kovalenko, N. Marzari, M. Grioni, M. Chergui, *Phys. Rev. Lett.* **2019**, *124*, 206402.



Leonardo R. V. Buizza is a final-year Ph.D. student in condensed matter physics at the University of Oxford as part of the EPSRC Centre for Doctoral Training in New and Sustainable Photovoltaics. He previously completed M.Sc. in physics as part of the Natural Sciences Tripos at the University of Cambridge, graduating in 2017. His research focuses on the interaction between the composition and optoelectronic properties of novel metal-halide semiconductors, specializing in photoluminescence and terahertz spectroscopy. He also has a wider interest in the transition to a net-zero energy system and the role of materials innovation in decarbonization.



Laura M. Herz is a Professor of Physics at the University of Oxford where she has led a research group since 2003. She received her Ph.D. in physics from the University of Cambridge in 2002 and was a Research Fellow at St John's College Cambridge from 2001 to 2003. Her research interests lie in the area of organic, inorganic and hybrid semiconductors, including aspects such as photophysical and nanoscale effects, self-assembly, charge-carrier dynamics, energy-transfer, and light-harvesting for solar energy conversion.